

SIMULATOR BASED EVALUATION OF ADAPTIVE ENVELOPE
PROTECTION ALGORITHMS FOR ACTIVE SIDESTICK CONTROLLERS

A THESIS SUBMITTED TO
THE GRADUATE SCHOOL OF NATURAL AND APPLIED SCIENCES
OF
MIDDLE EAST TECHNICAL UNIVERSITY

BY

ZEYNEP ÜNAL

IN PARTIAL FULFILLMENT OF THE REQUIREMENTS
FOR
THE DEGREE OF MASTER OF SCIENCE
IN
AEROSPACE ENGINEERING

AUGUST 2019

Approval of the thesis:

**SIMULATOR BASED EVALUATION OF ADAPTIVE ENVELOPE
PROTECTION ALGORITHMS FOR ACTIVE SIDESTICK CONTROLLERS**

submitted by **ZEYNEP ÜNAL** in partial fulfillment of the requirements for the degree of **Master of Science in Aerospace Engineering Department, Middle East Technical University** by,

Prof. Dr. Halil Kalıpçılar
Dean, Graduate School of **Natural and Applied Sciences**

Prof. Dr. İsmail Hakkı Tuncer
Head of Department, **Aerospace Engineering**

Assoc. Prof. Dr. İlkey Yavrucuk
Supervisor, **Aerospace Engineering, METU**

Examining Committee Members:

Prof. Dr. Ozan Tekinalp
Aerospace Engineering, METU

Assoc. Prof. Dr. İlkey Yavrucuk
Aerospace Engineering, METU

Prof. Dr. Kemal Leblebicioğlu
Electrical and Electronics Engineering, METU

Assist. Prof. Dr. Ali Türker Kutay
Aerospace Engineering, METU

Assist. Prof. Dr. Kutluk Bilge Arıkan
Mechanical Engineering, TED University

Date:

I hereby declare that all information in this document has been obtained and presented in accordance with academic rules and ethical conduct. I also declare that, as required by these rules and conduct, I have fully cited and referenced all material and results that are not original to this work.

Name, Surname: Zeynep Ünal

Signature :

ABSTRACT

SIMULATOR BASED EVALUATION OF ADAPTIVE ENVELOPE PROTECTION ALGORITHMS FOR ACTIVE SIDESTICK CONTROLLERS

Ünal, Zeynep

M.S., Department of Aerospace Engineering

Supervisor: Assoc. Prof. Dr. İlkey Yavrucuk

August 2019, 69 pages

In this thesis, a simulator environment with an active control system is developed for testing different force feedback maps for flight envelope limit avoidance. Previously developed flight envelope protection algorithm; named direct adaptive limit margin estimation method is improved with Single Hidden Layer Neural Network. Neural network based adaptive models are developed online using concurrent learning algorithm for weight update laws. Concurrent learning method uses both current data and recorded past data for adaptation. In this study, a Linear Parameter Neural Network and a Single Hidden Layer Neural Network are utilized and compared. The performance of single hidden layer neural network estimates are found to be more accurate for model error compensation. Three different force feedback maps are designed for pilot cueing with active side stick. Proposed force maps are tested on simulator environment. Performance of different force maps found to be dependent on type of limit parameters. Simulator based tests are conducted for rotorcraft model load factor limit avoidance and fixed wing aircraft load factor and angle of attack limit avoidance.

Keywords: Flight Envelope Protection, Carefree Maneuvering, Active Controls, Concurrent Learning, Neural Network, Adaptive Estimation

ÖZ

AKTİF JOYSTİCK KONTROLLER İÇİN ADAPTİF UÇUŞ ZARFI KORUMA ALGORİTMALARININ SİMULATOR TABANLI DEĞERLENDİRMESİ

Ünal, Zeynep

Yüksek Lisans, Havacılık ve Uzay Mühendisliği Bölümü

Tez Yöneticisi: Doç. Dr. İlkey Yavrucuk

Ağustos 2019 , 69 sayfa

Bu tezde uçuş zarfı koruması için aktif kontroller kullanılmış ve farklı pilot geri bildirim algoritmaları simulator ortamında denenmiştir. Daha önce geliştirilmiş olan adaptif limit marjini tahmin etme yöntemi tek katmanlı yapay sinir ağı kullanılarak geliştirilmiştir. Yapay sinir ağı tabanlı adaptif modellerde eş zamanlı öğrenme algoritması kullanılmıştır. Eş zamanlı öğrenme yöntemi, adaptasyon için hem anlık verileri hem de geçmişte kaydedilmiş verileri kullanır. Bu çalışmada adaptif eleman olarak hem lineer parameterli yapay sinir ağı hem de tek saklı katmanlı yapay sinir ağı kullanılmış ve karşılaştırılmıştır. Tek saklı katmanlı yapay sinir ağının performansı model hatasının telafisi ve parametre tahmini için daha doğru sonuçlar verdiği saptanmıştır. Aktif joystick ile pilot uyarısı için üç farklı pilot geri bildirim tasarlanmıştır. Önerilen geri bildirimler simulator ortamında test edilmiştir. Farklı geri bildirimlerin performansının limit parameteresinin türüne bağlı olduğu saptanmıştır. Helikopterde g-faktörü limitinden kaçınma ve sabit kanatlı uçak g-faktörü ve hücum açısı limitlerinden kaçınma testleri simulator ortamında yapılmıştır.

Anahtar Kelimeler: Uçuş Zarfı Koruma, Aktif Kontroller, Eş Zamanlı Öğrenme, Yapay Sinir Ağı

Babama...

ACKNOWLEDGMENTS

First and foremost, I would like to express my deepest gratitude to my supervisor Dr. Ilkay Yavrucuk for his support, advice and patient guidance. His courses on flight mechanics and controls inspired me to study further in this area and I cannot thank him enough for offering me his full support in my senior year when I was lost and hopeless. Through his guidance, not only have I improved my technical knowledge but also I have grown as a person. I am also grateful to him for always being kind, understanding and carefree that made working with him a breeze!

I want to emphasize my thanks to Gönenç Gürsoy. Without his guidance and assistance this thesis would not have been possible. I also would like to deliver my special thanks to my lab partner Bulut Efe Akmenek. Without him working on simulator would not be half as much fun. I am grateful to him for teaching me how to operate the simulator test bench for over 100 times and piloting difficult maneuvers for me.

I am particularly grateful to Metehan Yayla for his endless guidance, endless support, endless lectures on adaptive control and Lyapunov theory and our endless discussions. I feel lucky to witness his genius and benefit from his most valuable mentorship.

I would also like to thank my committee members Dr. Ozan Tekinalp, Dr. Kemal Leblebicioğlu, Dr. Ali Türker Kutay, and Dr. Kutluk Bilge Arıkan for their valuable suggestions and insights on this work.

I wish to thank Dr. Utku Kanoğlu for his support, guidance and numerous PhD. recommendation letters he has written for me. I also wish to thank him for the great course of AE501 we gave together. Studying partial differential equations with him had been a great escape at difficult times.

I want to offer my thanks to Aerotim Engineering. Not only have they fixed all the problems I had in the lab but also they have invited me to all their company parties.

I would like to thank my co-workers in the Aerospace Engineering department, espe-

cially Zalımlar Collection for great lunches and tea times. I also want to express my gratitude to my room mate Hazal Altuğ for her mentorship in my studies, in my work life and in my relationship with professors. Without her, I would still be thinking on what to write on some trivial e-mail.

My special thanks are extended to all my friends who are members of following Whatsapp groups: Starbakscılar, Goygoycular, İkeacılar, Havuzcular, Toyga Çorba, Işık dağcılar, Adhdnagsvdnanv, Patenci çetesi, RYOcular, Sağlıklı yaşama çelinc, Identificationcılar, and EE555ciler.

I am grateful to The ÜNAL Team for their never ending support and our not so frequent meetings. They are more than friends, they are family. (So they are included in the last paragraph as well!)

Last but not least, I would like to express my deepest gratitude to my family and within them Bahadır Bilgin for their love and support. Without them any success would be meaningless.

TABLE OF CONTENTS

ABSTRACT	v
ÖZ	vii
ACKNOWLEDGMENTS	x
TABLE OF CONTENTS	xii
LIST OF TABLES	xv
LIST OF FIGURES	xvi
LIST OF ABBREVIATIONS	xix
CHAPTERS	
1 INTRODUCTION	1
1.1 Motivation and Problem Definition	1
1.2 Flight Envelope Protection in Literature	1
1.3 Focus and Objective of Thesis	3
1.4 Contribution	4
1.5 Organization of the Thesis	4
2 METHODOLOGY	5
2.1 Introduction	5
2.2 Flight Envelope Protection Preliminaries	5
2.3 Direct Adaptive Limit Margin Estimation	8

2.3.1	Problem Definition	9
2.4	Adaptive Neural Network Augmentation	14
2.4.1	Concurrent Learning Preliminaries	14
2.4.2	Single Hidden Layer Neural Network Implementation	15
3	IMPLEMENTATION TO FLIGHT SIMULATOR	19
3.1	Introduction	19
3.2	Simulation Test Bench	19
3.2.1	Hard Stop Scheme	20
3.2.2	Soft Stop Scheme	21
3.2.3	Force Gradient	22
3.3	Application for a Rotorcraft	22
3.3.1	Problem Formulation	23
3.3.2	Adaptive Neural Network Augmentation with SHL Concurrent Learning	26
3.3.3	Simulation Results for Helicopter Load Factor Protection	28
3.3.3.1	Case 1 : Adaptive Control Limit Estimation	28
3.3.3.2	Case-2 : Limit Avoidance with Active Side Stick	34
3.4	Application for a Fixed Wing Aircraft	39
3.4.1	Problem Formulation	43
3.4.1.1	Load Factor as the Critical Limit Parameter	44
3.4.1.2	Angle of Attack as the Critical Limit Parameter	45
3.4.2	Adaptive Neural Network Augmentation with SHL Concurrent Learning	46
3.4.3	Simulation Results for Fixed Wing Aircraft Application	47

3.4.4	Case 1 : Adaptive Control Limit Estimation	48
3.4.5	Case 2 : Hard Stop	48
3.4.5.1	High Angle of Attack Turn	52
3.4.5.2	High Load Factor Turn	55
3.4.6	Case 3 : Soft Stop	55
3.4.6.1	High Angle of Attack Turn	57
3.4.6.2	High Load Factor Turn	60
4	CONCLUSIONS	63
	REFERENCES	67
	APPENDICES	

LIST OF TABLES

TABLES

LIST OF FIGURES

FIGURES

Figure 2.1	Flight Envelope Boundaries and Limits	6
Figure 2.2	Types of Limit Parameters	7
Figure 2.3	Tactile Cue Map Example	8
Figure 2.4	Limit Margin and Control Margin	9
Figure 2.5	Direct Adaptive Limit Margin Estimation	13
Figure 2.6	Single Hidden Layer Neural Network	15
Figure 3.1	Simulator Test Bench	20
Figure 3.2	Hard Stop Force Profile	21
Figure 3.3	Soft Stop Force Profile	22
Figure 3.4	Force Gradient Profile	23
Figure 3.5	Force Map	24
Figure 3.6	Simulation Block Diagram	24
Figure 3.7	Load Factor and Control Margins, Case-1, LPNN	29
Figure 3.8	Model Error and Singular Value, Case-1, LPNN	30
Figure 3.9	Helicopter States, Case-1, LPNN	31
Figure 3.10	Weights and Sensitivity, Case-1, LPNN	32

Figure 3.11	Aggressive Input, Case-1, LPNN	32
Figure 3.12	Load Factor and Control Margins, Case-1, SHL NN	33
Figure 3.13	Model Error and Singular Value, SHL NN, Case-1	33
Figure 3.14	Weights, SHL NN, Case-1	34
Figure 3.15	Aggressive Input, SHL NN, Case-1	35
Figure 3.16	Load Factor and Control Margins, Case-2, LPNN	36
Figure 3.17	Stick Force, Case-2, LPNN	36
Figure 3.18	Model Error and Singular Value, Case-2, LPNN	37
Figure 3.19	Load Factor and Control Margins, Case-2, SHL NN	37
Figure 3.20	Stick Force, Case-2, SHL NN	38
Figure 3.21	Model Error and Singular Value, Case-2, SHL NN	38
Figure 3.22	Load Factor and Control Margins for 60 kt Forward Flight	39
Figure 3.23	Model Error and Singular Value for 60 kt Forward Flight	40
Figure 3.24	Load Factor and Control Margins for 1734 fpm Climb	40
Figure 3.25	Model Error and Singular Value for 1734 fpm Climb	41
Figure 3.26	Load Factor and Control Margins for 1350 fpm Descend	41
Figure 3.27	Model Error and Singular Value for 1350 fpm Descend	42
Figure 3.28	Simulation Block Diagram	43
Figure 3.29	Case 1: Aircraft States	49
Figure 3.30	Case 1: Limit Parameters	50
Figure 3.31	Case 1: Elevator Input and Control Limits	50
Figure 3.32	Case 1: Adaptive Weights	51

Figure 3.33	Case 1: Model Error and Adaptive Element	51
Figure 3.34	Case 2: Aircraft States for High α Turn	52
Figure 3.35	Case 2: Limit Parameters for High α Turn	53
Figure 3.36	Case 2: Elevator Input and Control Limits for High α Turn	53
Figure 3.37	Case 2: Stick Force Feedback for High α Turn	54
Figure 3.38	Case 2: Weights for High α Turn	54
Figure 3.39	Case 2: Model Error and Adaptive Element for High α Turn	55
Figure 3.40	Case 2: Limit Parameters for High n_z Turn	56
Figure 3.41	Case 2: Elevator Input and Control Limits for High n_z Turn	56
Figure 3.42	Case 2: Stick Force Feedback for High n_z Turn	57
Figure 3.43	Case 3: Aircraft States for High α Turn	58
Figure 3.44	Case 3: Limit Parameters for High α Turn	58
Figure 3.45	Case 3: Elevator Input and Control Limits for High α Turn	59
Figure 3.46	Case 3: Stick Force Feedback for High α Turn	59
Figure 3.47	Case 3: Weights for High α Turn	60
Figure 3.48	Case 3: Model Error and Adaptive Element for High α Turn	61
Figure 3.49	Case 3: Limit Parameters for High n_z Turn	61
Figure 3.50	Case 3: Elevator Input and Control Limits for High n_z Turn	62
Figure 3.51	Case 3: Stick Force Feedback for High n_z Turn	62

LIST OF ABBREVIATIONS

AFCS	Automatic Flight Control System
SAS	Stability Augmentation System
PID	Proportional Integral Derivative
RPM	Revolutions per minute
SHL NN	Single Hidden Layer Neural Network
LPNN	Linear Parameter Neural Network
CL	Concurrent Learning
NGI	Next Generation Inceptor
ft	Feet
kt	Knots
fpm	Feet per minute
RBF NN	Random Basis Function Neural Network

CHAPTER 1

INTRODUCTION

1.1 Motivation and Problem Definition

An aircraft's flight regime is restricted by its limits. Aerodynamic, structural, power, control, and operational limits come together and form flight envelope boundaries. Within the flight envelope, operation of the vehicle is safe; however, violation of limits increase the risk of failure. Hence, for piloted aircraft its pilot's duty to monitor the limits during flight to ensure safety. Making pilots monitor the limiting parameters increases pilot work load and decreases the operational flight envelope, as humans tend to be conservative while avoiding limits. Flight envelope protection systems ensure that the aircraft stays within envelope boundaries and aim to reduce pilot workload and maximize the operational flight envelope.

Testing flight envelope protection algorithms in real life scenarios is essential to show effectiveness. In this study a simulator environment is set to test envelope protection algorithms. The simulator test bench consists of an active inceptor to cue pilots against envelope limits. One of the important factors in effective limit avoidance is the design of the force feel of the active inceptor. Thus, different force feedback maps are designed and tested.

1.2 Flight Envelope Protection in Literature

Flight envelope protection algorithms can be grouped in two subcategories. First one is flight envelope protection by manipulation of controller gains. This approach utilizes an automatic flight control system (AFCS) or a stability augmentation system

(SAS) for envelope protection. Second approach is flight envelope protection by pilot cueing. Pilot cueing is a warning system that increase situational awareness of the pilot and handling quality of the aircraft.

Flight envelope protection with automatic flight control systems is first introduced in 1987 for load factor limit avoidance [20] where the automatic flight control system for a fighter aircraft limits parameters, such as acceleration, velocity, and attitude, such that the limit design loads are not exceeded. Similarly, in [21] automatic flight control systems is used for load factor protection for supersonic fighter aircraft. Later, a similar approach is applied to Airbus A320, feedback laws are employed for load factor and angle of attack protection [6]. Same approach is also applied to rotorcraft; in [15] AFCS laws are modified to maintain hub moments within structural limits. In more recent studies, [23, 22] a method utilizing PID control and potential functions for bank angle protection is proposed. The downside of envelope protection with control gain manipulation is that, it restricts pilot authority. Furthermore, design of such control laws requires complete information on aircraft model which can only be obtained through flight tests.

Pilot cueing is another approach in flight envelope protection which gives the pilot more authority. The aim of cues is to inform the pilot about the proximity of the vehicle to its limits. Cues could be aural, visual, tactile or combination of all. In earlier examples of pilot cueing visual cues are delivered through helmet mounted display and aural cues are given through pilot headset [16]. For aircraft with unconventional control surfaces or large cargo or passenger aircrafts it is impossible to operate with mechanically linked control surfaces. Therefore, fly-by-wire systems are employed in modern aircraft where pilot inputs are received through an active inceptor and delivered to the control surface actuator. Q feel systems can be employed to create an artificial feel of the aircraft. Q-feel systems use dynamic pressure measurements on control surfaces and convey that information to the pilot. Tactile cues are given through active inceptors as force feedback in fly-by-wire systems can also artificially create a "feel" of the aircraft to increase handling quality. In [24] tactile cueing is shown to be an effective means of informing the pilot on impending flight envelope exceedance. Similarly, in [25] effectiveness of use of active inceptors and conventional side stick for helicopter flight envelope protection is compared. Active inceptor performed better than conventional side stick for limit avoidance. [7] and [14] also

support that active inceptor is an effective flight envelope protection tool. Effectiveness of flight envelope protection systems with active inceptors can be enhanced if the tactile cues can be provided before the aircraft exceeds its limits. In [17], future values of RPM for a rotorcraft is estimated using collective input and current RPM value with a linear adaptive element. In [4] polynomial neural networks are used for main rotor hub moment and torque limit protection. Similarly, neural network based estimation algorithms are employed in [11] for future state estimations. This study also introduces the dynamic trim concept which is a maneuvering steady state condition for an aircraft. Dynamic trim condition is estimate by feeding large data sets into multilayer neural networks. Later, in [12] the method is named as Adaptive Dynamic Trim Estimation and improved adding an online trained neural network. In [27, 26] online limit and control margin estimation is enabled with limited information on plant. In these studies online parameter estimation is done through iterations. Then, the method given in [27, 26] is enhanced with concurrent learning augmentation in [9, 10]. With concurrent learning augmentation, limit parameters can be estimated without online iterations [8]; thus, the method is named as Direct Adaptive Limit Margin Estimation.

1.3 Focus and Objective of Thesis

In this thesis the direct adaptive limit margin estimation method introduced in [8, 10] is employed. For a given nonlinear model, states are estimated as the summation of approximate inverse model and an adaptive element. The adaptive element is a neural network scheme that uses concurrent learning as its learning algorithm. Concurrent learning uses recorded data to adapt without persistent excitation [5]. Both linear parameter neural network (LPNN) and single hidden layer neural network (SHL NN) are used in this study. Estimated future states are directly used in limit margin calculations. For control margin calculations, a linear relationship between limit margin and control margin is established. Then, the estimated control limits are fed into active side stick given in [3] for flight envelope protection with pilot cueing. The method is tested on a simulator test bench for different force feedback maps.

1.4 Contribution

Contributions of this thesis are as follows:

- A simulator environment is set and proved to be sufficient for analyzing new envelope protection algorithms.
- The adaptive learning performance of the given method [10] is enhanced with single hidden layer neural network concurrent learning augmentation.
- Limit avoidance with direct adaptive limit margin estimation method is evaluated in simulator environment with active side stick for both rotorcraft and fixed wing aircraft platforms.
- The active inceptor is enabled to provide different force feedback cues and various force maps are designed and tested on simulator.

1.5 Organization of the Thesis

This thesis is organized as follows: In Chapter 2 basic concepts in flight envelope protection systems are introduced. Then, the control margin estimation method namely "Direct Adaptive Limit Margin Estimation Method" given in [10] is explored. Explanations on Concurrent Learning (CL) method for weight update laws in linear parameter neural network and single hidden layer neural network are also presented in Chapter 2. In Chapter 3 implementation of the proposed method to a flight simulator is presented. The properties of the flight simulator are provided. Then, details on helicopter load factor limit avoidance application and load factor and angle of attack limit avoidance implementation for fixed wing aircraft are explained. Finally, simulation results are presented. Conclusions are delivered in Chapter 4.

CHAPTER 2

METHODOLOGY

2.1 Introduction

This chapter is divided into two parts. First, in section 2.2 basic concepts in flight envelope protection systems are introduced. Then, in section 2.3 a control margin estimation method namely "Direct Adaptive Limit Margin Estimation Method" is explored. Some preliminary concepts for the method are briefly discussed for a general case with full state measurement and also for a less general case with a linear approximate model. Direct adaptive limit margin estimation method includes an adaptive element for uncertainty estimations. In section 2.4 adaptive neural network schemes that can be implemented in limit margin estimation are explained. This study employs Concurrent Learning (CL) method for weight update laws in neural network. After introducing Linear Parameter Neural Network Concurrent Learning (LPNN CL) scheme, in section 2.4.2 Single Hidden Layer Neural Network Concurrent Learning (SHL NN CL) scheme is explained.

2.2 Flight Envelope Protection Preliminaries

Limits of an aircraft, such as aerodynamic, structural, power limits, etc. form the aircraft's flight envelope (Fig. (2.1)). Operation is safe within this envelope and risk of failure increases when the envelope boundaries are violated. *Limit parameter*, is a term used for states or parameters that limit the flight envelope. Limit parameters are grouped based on their response types [26]. Some of the limit parameter types are listed below:

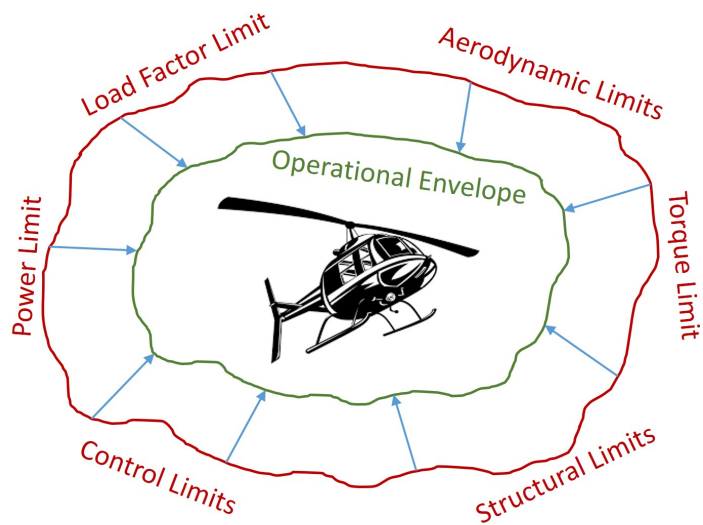


Figure 2.1: Flight Envelope Boundaries and Limits

- *Peak Response Critical* limit parameters exceed their maximum value during transient response. Some examples to this kind of limit parameters are hub moments or flapping in rotorcraft. (Fig. (2.2a))
- *Steady State Critical* limit parameters exceed their limit at their steady state response. Angle of attack is an example of this kind of limit parameters. (Fig. (2.2b))
- For *Peak and Steady State Critical* limit parameters both transient response and steady state response are critical. (Fig. (2.2c))
- *Integral Response Critical* limit parameters do not have a steady state or peak value. Bank angle is an integral response critical type limit parameter.(Fig. (2.2d))

Pilots need to monitor limit parameters during flight in order to avoid violating flight envelope boundaries. Not only this increases the pilot workload but also shrinks operational envelope since humans have a tendency to be conservative while avoiding limits(Fig. (2.1)). Flight envelope protection systems aim to reduce pilot workload and maximize operational flight envelope. Flight envelope protection systems can be divided into two sub categories: Automatic flight envelope protection systems

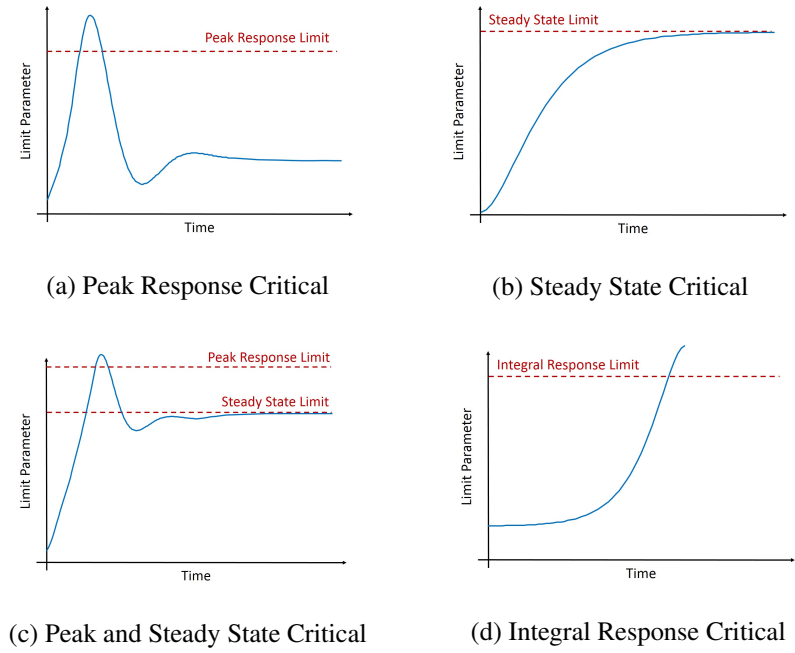


Figure 2.2: Types of Limit Parameters

and pilot cueing. Automatic flight envelope protection systems employ a computer to calculate and impose the necessary control input to avoid limits automatically. Downside of this approach is limited pilot authority. Pilot cueing, on the other hand is a warning system that gives pilots more authority. Cues can be visual, aural, tactile or combination of these. These cues must be initiated before the envelope boundaries are violated so that the pilot can be warned in time. This study focuses on tactile cues. Tactile cues are given through programmable active inceptors. An example of a tactile cue design is given in Fig. (2.3). Here, x -axis is the stick angle and y -axis is the stick force. δ_{min} and δ_{max} are the stick angles at lower limit and upper limit respectively. Within safe operational range no force is exerted on the active inceptor. As the vehicle approaches its envelope limits, force on the stick increases so that the envelope boundaries are not violated. The stick angles that correspond to the envelope limits (δ_{min} and δ_{max}) are unknown and time varying parameters that are also known as the *control limits*. In order to give timely tactile cues, control limits must be accurately estimated through their relation with the limit parameter. Limit margin and control margin concepts are demonstrated in Fig. (2.4). *Limit margin* is defined as the proximity of a limit parameter to the envelope boundaries. The

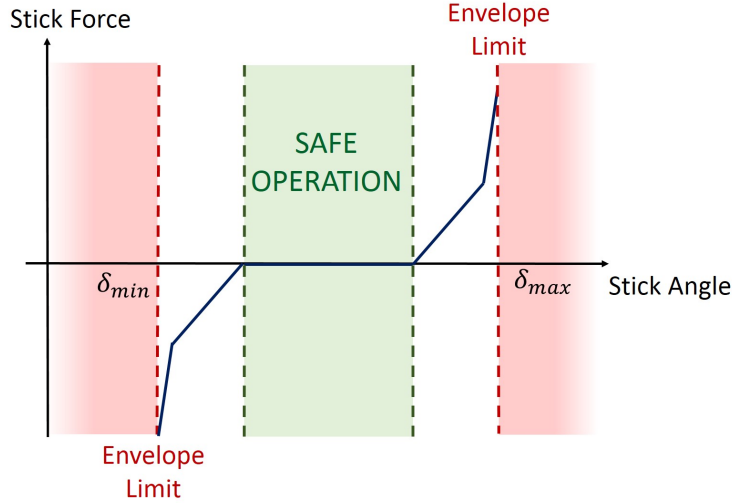


Figure 2.3: Tactile Cue Map Example

allowable control travel that would result in limit violation is defined as the *control margin*. Control margin can also be defined as the distance between corresponding control input and the *control limit*. The limit margin is estimated using an estimation of future states so that the tactile cues can be initiated before the vehicle reaches its limits. Then, establishing a relationship between limit margin and control margin allowable control travels are estimated. When control limits are known, tactile cues can be initiated as the pilot input approaches the control limits. Details on the limit margin estimation method will be provided in the following section.

2.3 Direct Adaptive Limit Margin Estimation

Direct Adaptive Limit Margin Estimation Method given in [10] is explained here. For a given nonlinear model, states are estimated as the summation of approximate inverse model and an adaptive element. The derivative terms in inverse model are approximated using central difference relations at delayed time step. Then, the state estimate can be directly used in limit margin calculations. Next, steady state value of the limit parameter is found by inserting zeros to derivative terms. For control margin calculations, a linear relationship between limit margin and control margin is established. This linear relationship is based on control sensitivity, which is the

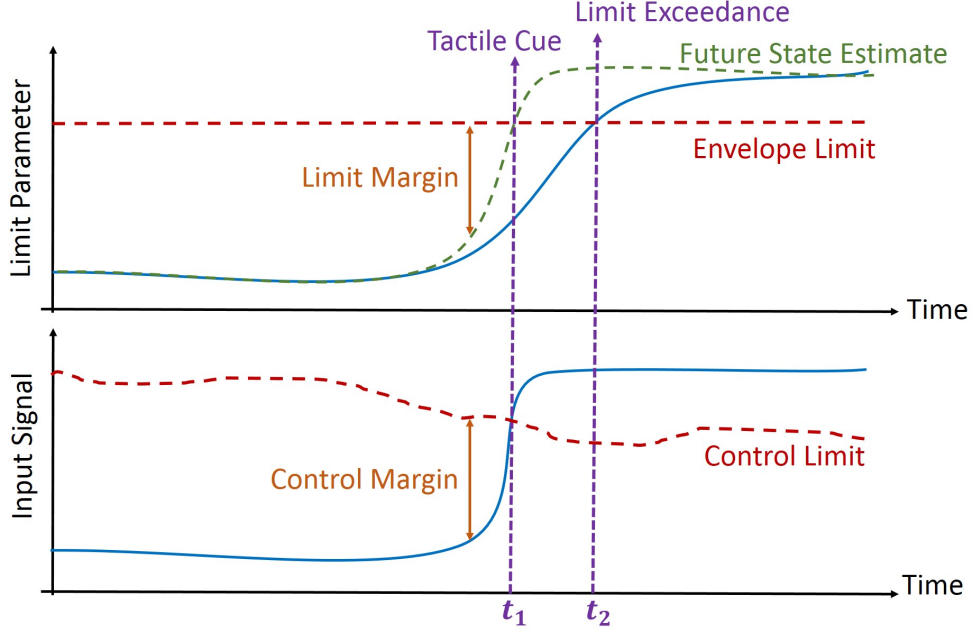


Figure 2.4: Limit Margin and Control Margin

derivative of the steady state limit parameter with respect to control input.

2.3.1 Problem Definition

Consider the nonlinear system:

$$\dot{\mathbf{x}} = \mathbf{f}(\mathbf{x}, \mathbf{u}) \quad \mathbf{x}(t_0) = \mathbf{x}_0 \quad (21)$$

where, the state vector $\mathbf{x} \in \mathfrak{R}^{n \times 1}$ has a known initial condition \mathbf{x}_0 . The known control input vector is given as $\mathbf{u} \in \mathfrak{R}^{p \times 1}$. The vector function $\mathbf{f} : \mathfrak{R}^{n \times p} \rightarrow \mathfrak{R}^{n \times 1}$ is assumed to be continuous and satisfy global Lipschitz condition.

The state vector can be expressed as [27]:

$$\mathbf{x} = \begin{bmatrix} \mathbf{x}_f & \mathbf{x}_s \end{bmatrix}^T \quad (22)$$

where, $\mathbf{x}_f \in \mathfrak{R}^{l \times 1}$ represent fast states such as angular rates, and angle of attack and $\mathbf{x}_s \in \mathfrak{R}^{(n-l) \times 1}$ represent slow states such as forward speed and Euler angles of the system.

The limit margin is the difference between the envelope limit and the fast states [27]:

$$\mathbf{x}_{f_{marg}} = \mathbf{x}_{f_{lim}} - \mathbf{x}_f \quad (23)$$

Similarly, control margin is defined as:

$$\mathbf{u}_{marg} = \mathbf{u}_{lim} - \mathbf{u} \quad (24)$$

Assuming the envelope limits in Eq. (23) are given, the aim is to calculate control limits in Eq. (24) by estimating control margins and to cue the pilot before the vehicle reaches its limits.

Assuming fast states, slow states and input are all measured, dynamics of fast states can be represented as a function of fast states themselves \mathbf{x}_f , slow states \mathbf{x}_s , and the control input \mathbf{u} [27]:

$$\dot{\mathbf{x}}_f = \mathbf{f}_1(\mathbf{x}_f, \mathbf{x}_s, \mathbf{u}) \quad (25)$$

Assume, \mathbf{f}_1 is invertible and \mathbf{f}_1^{-1} be the inverse of fast state dynamics. Then, fast states can be expressed as:

$$\mathbf{x}_f = \mathbf{f}_1^{-1}(\dot{\mathbf{x}}_f, \mathbf{x}_s, \mathbf{u}) \quad (26)$$

However, fast state dynamics of the actual plant, \mathbf{f}_1 is rarely invertible or even available. Therefore, instead of \mathbf{f}_1^{-1} the inverse of fast state dynamics, an approximated model inverse, $\hat{\mathbf{f}}_1^{-1}$ is used together with the modeling error $\boldsymbol{\xi}$ to express fast states of the plant [10].

$$\mathbf{x}_f = \hat{\mathbf{f}}_1^{-1}(\dot{\mathbf{x}}_f, \mathbf{x}_s, \mathbf{u}) + \boldsymbol{\xi} \quad (27)$$

The modeling error $\boldsymbol{\xi}$ in Eq. (27) can be estimated with an adaptive element, $\boldsymbol{\Delta}$, and estimate of fast state $\hat{\mathbf{x}}_f$ becomes:

$$\hat{\mathbf{x}}_f = \hat{\mathbf{f}}_1^{-1}(\dot{\hat{\mathbf{x}}}_f, \mathbf{x}_s, \mathbf{u}) + \boldsymbol{\Delta}(\dot{\hat{\mathbf{x}}}_f, \mathbf{x}_s, \mathbf{u}) \quad (28)$$

The model tracking error e is obtained by subtracting Eq. (27) from Eq. (28):

$$e = \boldsymbol{\xi} - \boldsymbol{\Delta}(\dot{\hat{\mathbf{x}}}_f, \mathbf{x}_s, \mathbf{u}) \quad (29)$$

Ideally, $\boldsymbol{\xi}$ and $\boldsymbol{\Delta}$ would cancel each other and the model tracking error e would be zero. In reality, $\boldsymbol{\Delta}$ is trained online such that e is minimized.

The derivative term, $\dot{\hat{\mathbf{x}}}_f$, in Eq. (28) may not be available in current time. Hence, states derivatives are obtained at delayed time step as described in [10] using central

difference method.

The central difference operator, $\partial(\cdot)_d : \mathfrak{R}^{l \times 1} \rightarrow \mathfrak{R}^{l \times k}$ takes a vector as the input and its output is a matrix of central differences at delayed time step, d . Where, $l \in \mathfrak{N}^+$ is the size of the input vector and $k \in \mathfrak{N}^+$ is the number of central differences.

$$\partial(\cdot)_d = \begin{bmatrix} (\cdot)_{d+1} - (\cdot)_{d-1} & (\cdot)_{d+2} - (\cdot)_{d-2} & \dots & (\cdot)_{d+k} - (\cdot)_{d-k} \end{bmatrix} \quad (210)$$

The average central difference operator, $\bar{\partial} : \mathfrak{R}^{l \times 1} \rightarrow \mathfrak{R}^{l \times 1}$ calculates the average sum of central differences:

$$\bar{\partial}(\cdot)_d = \frac{1}{k} \sum_{i=1}^k \partial(\cdot)_d(:, i) \quad (211)$$

The Eq. (28) can be rewritten at delayed time step as:

$$\hat{\mathbf{x}}_{f_d} = \hat{\mathbf{f}}_1^{-1}(\dot{\mathbf{x}}_{f_d}, \mathbf{x}_{s_d}, \mathbf{u}_d) + \Delta(\dot{\mathbf{x}}_{f_d}, \mathbf{x}_{s_d}, \mathbf{u}_d) \quad (212)$$

The state derivative at delayed time step, $\dot{\mathbf{x}}_{f_d}$ in model inverse term in Eq. (212) is estimated using the average central difference operator such that, $\dot{\mathbf{x}}_{f_d} = \bar{\partial}(\mathbf{x}_f)_d$. The central difference matrix, $\partial(\mathbf{x}_f)_d$ is fed into the adaptive element in Eq. (212). The adaptive element not only compensates for the model error, ξ but also the error caused by state derivative estimations [10].

Fast states can be estimated at delayed time step as:

$$\hat{\mathbf{x}}_{f_d} = \hat{\mathbf{f}}_1^{-1}(\bar{\partial}(\mathbf{x}_f)_d, \mathbf{x}_{s_d}, \mathbf{u}_d) + \Delta(\partial(\mathbf{x}_f)_d, \mathbf{x}_{s_d}, \mathbf{u}_d) \quad (213)$$

The model tracking error at delayed time becomes:

$$\mathbf{e}_d = \boldsymbol{\xi}_d - \Delta(\partial(\mathbf{x}_f)_d, \mathbf{x}_{s_d}, \mathbf{u}_d) \quad (214)$$

During a maneuver, fast states reach their steady state condition before slow states reach theirs. Dynamic trim is the condition where fast states have reached their steady state values [27]:

$$\dot{\mathbf{x}}_f = 0 \quad (215)$$

Using the central difference operators, dynamic trim can also be expressed at delayed time as:

$$\bar{\partial}(\mathbf{x}_f)_d = 0 \quad (216)$$

When the dynamic trim condition in Eq. (216) is inserted in Eq. (213) fast states at dynamic trim can be estimated at current time step provided that adaptive weights

have converged to their optimal values [10].

$$\hat{\mathbf{x}}_{f_{DT}} = \hat{\mathbf{f}}_1^{-1}(0, \mathbf{x}_s, \mathbf{u}) + \mathbf{\Delta}(0, \mathbf{x}_s, \mathbf{u}) \quad (217)$$

A special case to the direct limit margin estimation method is when the approximate model is selected as a linear model:

$$\dot{\mathbf{x}}_f = A_1 \mathbf{x}_f + A_2 \mathbf{x}_s + B \mathbf{u} \quad (218)$$

Then, fast state estimate in Eq. (212) at delayed time step becomes:

$$\hat{\mathbf{x}}_{f_d} = -A_1^{-1}(-\dot{\mathbf{x}}_{f_d} + A_2 \mathbf{x}_{s_d} + B \mathbf{u}_d) + \mathbf{\Delta}(\dot{\mathbf{x}}_{f_d}, \mathbf{x}_{s_d}, \mathbf{u}_d) \quad (219)$$

Using the central difference and average central difference operators the fast state estimate becomes:

$$\hat{\mathbf{x}}_{f_d} = -A_1^{-1}(-\bar{\mathbf{\partial}}(\mathbf{x}_f)_d + A_2 \mathbf{x}_{s_d} + B \mathbf{u}_d) + \mathbf{\Delta}(\bar{\mathbf{\partial}}(\mathbf{x}_f)_d, \mathbf{x}_{s_d}, \mathbf{u}_d) \quad (220)$$

Inserting the condition in Eq. (216), dynamic trim at current time becomes:

$$\hat{\mathbf{x}}_{f_{DT}} = -A_1^{-1}(A_2 \mathbf{x}_{s_d} + B \mathbf{u}_d) + \mathbf{\Delta}(0, \mathbf{x}_{s_d}, \mathbf{u}_d) + \mathbf{e}_d \quad (221)$$

Dynamic trim limit margin can be defined as the difference between envelope limit and the dynamic trim value of the limiting parameter. This is the measure of how far from the limit the vehicle will be at steady state.

$$\mathbf{x}_{f_{marg,DT}} = \mathbf{x}_{f_{lim}} - \hat{\mathbf{x}}_{f_{DT}} \quad (222)$$

In Eq. (222) it is assumed that envelope limits for the vehicle are known; thus, limit margins can be calculated. On the other hand, in Eq. (24), both control limits and control margins are unknown.

A linear relationship between limit margin and control margin established by control sensitivity, $\mathbf{S} \in \mathbb{R}^{l \times 1}$ in [10]:

$$\mathbf{u}_{marg,DT} = \text{diag}(\mathbf{S} \mathbf{I}_v)^{-1} \mathbf{x}_{f_{marg,DT}} \quad (223)$$

Where, $\mathbf{I}_v = [1 \ 1 \ 1 \ \dots \ 1]^T$ and control sensitivity, \mathbf{S} is defined as the derivative of the dynamic trim estimation of the state with respect to control input.

$$\mathbf{S} = \frac{\partial \hat{\mathbf{x}}_{f_{DT}}}{\partial \mathbf{u}} = \frac{\partial (\hat{\mathbf{f}}_1^{-1}(0, \mathbf{x}_s, \mathbf{u}) + \mathbf{\Delta}(0, \mathbf{x}_s, \mathbf{u}))}{\partial \mathbf{u}} \quad (224)$$

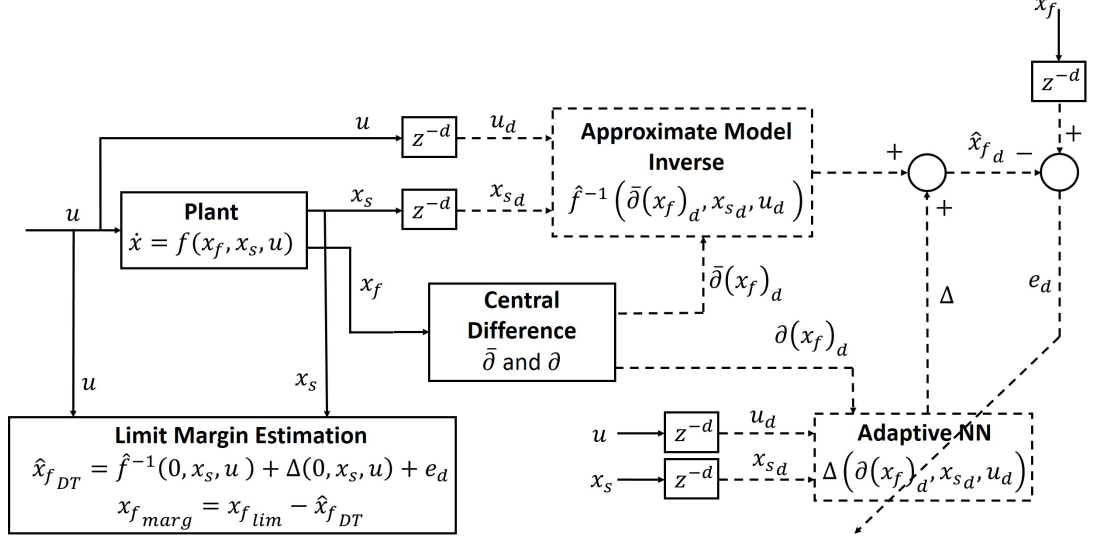


Figure 2.5: Direct Adaptive Limit Margin Estimation

In [10] conditions for $diag(\mathbf{S}\mathbf{I}_v)$ to be invertible are specified.

The control margin found in Eq. (223) can be inserted into Eq. (24) to calculate the control limits:

$$\mathbf{u}_{lim} = \mathbf{u}_{marg} + \mathbf{u} \quad (225)$$

$$\mathbf{u}_{lim} = diag(\mathbf{S}\mathbf{I}_v)^{-1} \mathbf{x}_{f_{marg,DT}} + \mathbf{u} \quad (226)$$

Some limit parameters may reach their limits during transient response. For peak response critical limit parameters Eq. (225) is slightly modified such that:

$$\mathbf{u}_{lim,upper} = \min(|diag(\mathbf{S}\mathbf{I}_v)^{-1} \mathbf{x}_{f_{marg}}|, |diag(\mathbf{S}\mathbf{I}_v)^{-1} \mathbf{x}_{f_{marg,DT}}|) + \mathbf{u} \quad (227)$$

$$\mathbf{u}_{lim,lower} = -\min(|diag(\mathbf{S}\mathbf{I}_v)^{-1} \mathbf{x}_{f_{marg}}|, |diag(\mathbf{S}\mathbf{I}_v)^{-1} \mathbf{x}_{f_{marg,DT}}|) + \mathbf{u} \quad (228)$$

Where, $diag(\mathbf{S}\mathbf{I}_v)^{-1} \mathbf{x}_{f_{marg}}$ is the instantaneous control limit calculated using instantaneous limit margin and $diag(\mathbf{S}\mathbf{I}_v)^{-1} \mathbf{x}_{f_{marg,DT}}$ is the steady state limit calculated using limit margin for dynamic trim condition. In Fig. (2.5) block diagram representation of Direct Adaptive Limit Margin Estimation Method is presented. In this figure dashed lines indicate calculations at delayed time step.

2.4 Adaptive Neural Network Augmentation

The adaptive element introduced in Eq. (28) is selected as Single Hidden Layer Neural Network (SHL NN) and the learning algorithm is Concurrent Learning (CL). Concurrent Learning is an adaptive learning scheme that uses recorded data for learning and does not require persistency of excitation [5]. This learning method is selected because of its global estimation property. In order to have accurate dynamic trim estimations and control limit estimations, optimal weights need to be found and used in calculations.

2.4.1 Concurrent Learning Preliminaries

For linearly parameterizable uncertainties the adaptive element Δ can be constructed as:

$$\Delta(\bar{x}) = W^T \Phi(\bar{x}). \quad (229)$$

where, $\bar{x} = [\mathbf{x}_s(t), \bar{\partial}(\mathbf{x}_f), u]^T \in \mathfrak{R}^{r \times 1}$ is the input vector to neural network, $W \in \mathfrak{R}^{m \times l}$ is the set of approximate weights and, $\Phi(\bar{x}) = [\phi_1(\bar{x}), \phi_2(\bar{x}), \dots, \phi_m(\bar{x})]$, where $\phi_i : \mathfrak{R}^{r \times 1} \rightarrow \mathfrak{R}$, $i = 1, 2, \dots, m$ are known and bounded activation functions.

Then, the model tracking error is given as [5]:

$$\mathbf{e} = \tilde{W}^T \Phi(\bar{x}) \quad (230)$$

where, $\tilde{W} = W^* - W$ is the error between the optimal and the approximate weights. In concurrent learning, online recorded data is used in weight update. For this approach, the model tracking error, \mathbf{e} , and the network basis, $\Phi(\bar{x})$, are recorded in an $m \times p$ history stack matrix, Z :

$$Z = [\Phi_1, \Phi_2, \Phi_3, \dots, \Phi_p]. \quad (231)$$

The data to be recorded is selected such that the minimum singular value of Z , $\sigma_{\min}(Z)$, is increased [5, 10].

The weight update law is determined using concurrent learning [5] as:

$$\dot{W}(t) = \Gamma(\Phi(\bar{x})\mathbf{e}^T + \sum_{j=1}^p \Phi_j(\bar{x})\mathbf{e}_j^T) \quad (232)$$

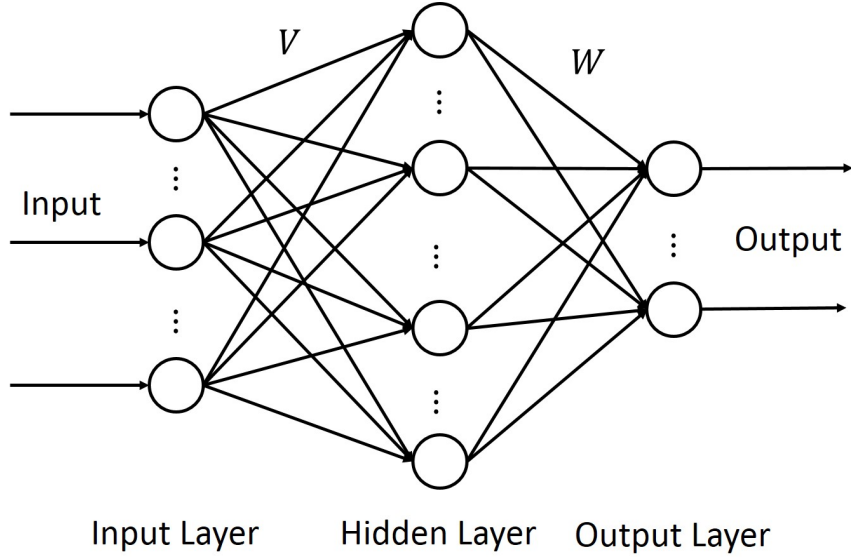


Figure 2.6: Single Hidden Layer Neural Network

where, Γ is a positive definite learning gain matrix. A proof of boundedness for the above weight update law is presented in [10].

2.4.2 Single Hidden Layer Neural Network Implementation

Uncertainties in nonlinear models may not be linearly parametrizable or structured. Single Hidden Layer Neural Networks (SHL NN) is a nonlinear map that can be used for approximating continuous unstructured uncertainties. Schematic representation of single hidden layer neural network is given in Fig. (2.6). The adaptive element Δ can be constructed as:

$$\Delta(\bar{\mathbf{x}}) = \mathbf{W}^T \sigma(\mathbf{V}^T \bar{\mathbf{x}}). \quad (233)$$

where; $\bar{\mathbf{x}} = [\mathbf{x}_s(t), \bar{\partial}(\mathbf{x}_f), u]^T \in \mathfrak{R}^{(r+1) \times 1}$ is the input vector to neural network, $\mathbf{W} \in \mathfrak{R}^{(m+1) \times l}$ and $\mathbf{V} \in \mathfrak{R}^{(r+1) \times m}$ are the synaptic weights that connect hidden layer to output layer and synaptic weights that connect input layer to hidden layer

respectively:

$$\mathbf{W} = \begin{bmatrix} \theta_{w,1} & \theta_{w,2} & \dots & \theta_{w,l} \\ w_{1,1} & w_{1,2} & \dots & w_{1,l} \\ \vdots & \vdots & & \vdots \\ w_{m,1} & w_{m,2} & \dots & w_{m,l} \end{bmatrix} \in \mathfrak{R}^{(m+1) \times l} \quad (234)$$

Here, $\theta_{w,i}$'s are bias terms and $w_{i,j}$ are synaptic weights. Similarly, the synaptic weight matrix between input layer and hidden layer is in the form:

$$\mathbf{V} = \begin{bmatrix} \theta_{v,1} & \theta_{v,2} & \dots & \theta_{v,m} \\ v_{1,1} & v_{1,2} & \dots & v_{1,m} \\ \vdots & \vdots & & \vdots \\ v_{r,1} & v_{r,2} & \dots & v_{r,m} \end{bmatrix} \in \mathfrak{R}^{(r+1) \times m} \quad (235)$$

Here, $\theta_{v,i}$'s are bias terms and $v_{i,j}$ are synaptic weights. The sigmoidal activation function vector is:

$$\boldsymbol{\sigma}(\mathbf{z}) = \begin{bmatrix} b_w \\ \sigma_1(z_1) \\ \sigma_2(z_2) \\ \vdots \\ \sigma_m(z_m) \end{bmatrix} \in \mathfrak{R}^{(m+1) \times 1} \quad (236)$$

with $\mathbf{z} = \mathbf{V}^T \bar{\mathbf{x}}$ and sigmoidal activation functions are given as:

$$\sigma_i(z_i) = \frac{1}{1 + e^{-a_i z_i}} \quad (237)$$

For concurrent learning, e , and the network basis, $\bar{\mathbf{x}}$ are recorded in history stack matrix and using the assumptions in [5] and minimizing singular value as described in [10]. The weight update law becomes [5]:

$$\dot{\mathbf{W}}(t) = \Gamma_W ((\sigma(\mathbf{V}^T \bar{\mathbf{x}}) - \sigma'(\mathbf{V}^T \bar{\mathbf{x}}) \mathbf{V}^T \bar{\mathbf{x}}) \mathbf{e}^T + W_c \sum_{j=1}^p (\sigma(\mathbf{V}^T \bar{\mathbf{x}}_j) - \sigma'(\mathbf{V}^T \bar{\mathbf{x}}_j) \mathbf{V}^T \bar{\mathbf{x}}_j) \mathbf{e}_j^T) \quad (238)$$

$$\dot{\mathbf{V}}(t) = \Gamma_V \bar{\mathbf{x}} \mathbf{e}^T \mathbf{W}^T \sigma'(\mathbf{V}^T \bar{\mathbf{x}}) + V_c \sum_{j=1}^p \bar{\mathbf{x}}_j \mathbf{e}_j^T \mathbf{W}^T \sigma'(\mathbf{V}^T \bar{\mathbf{x}}_j) \quad (239)$$

where;

$$W_c = I - \frac{(\sigma(\mathbf{V}^T \bar{\mathbf{x}}) - \sigma'(\mathbf{V}^T \bar{\mathbf{x}}) \mathbf{V}^T \bar{\mathbf{x}}) (\sigma(\mathbf{V}^T \bar{\mathbf{x}}) - \sigma'(\mathbf{V}^T \bar{\mathbf{x}}) \mathbf{V}^T \bar{\mathbf{x}})^T}{(\sigma(\mathbf{V}^T \bar{\mathbf{x}}) - \sigma'(\mathbf{V}^T \bar{\mathbf{x}}) \mathbf{V}^T \bar{\mathbf{x}})^T (\sigma(\mathbf{V}^T \bar{\mathbf{x}}) - \sigma'(\mathbf{V}^T \bar{\mathbf{x}}) \mathbf{V}^T \bar{\mathbf{x}})} \quad (240)$$

$$V_c = I - \frac{\bar{x}\bar{x}^T}{\bar{x}^T\bar{x}} \quad (241)$$

Boundedness proofs in [26] and [8] are applicable to above weight update law.

CHAPTER 3

IMPLEMENTATION TO FLIGHT SIMULATOR

3.1 Introduction

In this chapter, the method described in Chapter 2 is implemented to a flight simulator. In section 3.2 properties of the flight simulator are presented. One of the main components of the flight simulator is active side stick which is programmed to give force feedback cues to the pilots. Design of force feedback cues are explained in subsection 3.2.1 and subsection . The method is first applied to a rotorcraft model in section 3.3. In section 3.3.1 details on helicopter load factor limit avoidance application are explained. And simulation results are presented in section 3.3.3. Next, the method is applied to a fixed wing aircraft model in section 3.4. Load factor and angle of attack limit avoidance implementation for aircraft is explained in section 3.4.1. Finally, simulation results are presented in 3.4.3.

3.2 Simulation Test Bench

The simulator environment shown in Fig.3.1 consists of a Stirling Dynamics Next Generation Inceptor (NGI) [3] , Flight Link Advanced Helicopter Package [1], Saitek pilot controllers [2] and two desktop computers. Computers are connected to each other through TCP/IP connections. Flight Link Advanced Helicopter Package consists of a cyclic, collective, pedals and a pilot seat. For fixed wing configuration cyclic and collective are disconnected, instead Saitek pilot controllers are installed for throttle input. The Stirling Dynamics NGI is used as active side stick controller. The flight model runs in Simulink as an s-function. Therefore, all input and output relations are



Figure 3.1: Simulator Test Bench

established in Simulink. Another S-function in the flight model allows communication with the active controller. The lateral and longitudinal angles of the stick are read via this s-function and are fed into the flight model. The envelope protection algorithm inputs the desired force values for given a stick angle to the stick for continuous changes in the force profile. Also, stick vibration amplitude and frequency can be set from the flight model. Each time the force profile of the side stick needs a change, an array of force values and corresponding stick angles are sent to the controller. For this study three tactile cueing methods are used; hard stop, soft stop, and force gradient.

3.2.1 Hard Stop Scheme

Hard stop force profile is illustrated in Fig. (3.2). The active side stick exerts no force in nominal position. The side stick acts like a passive stick in safe operation region with a preset constant force profile. When the critical control margin is reached the active stick prevents any further movement in the limiting direction. The critical control margin is a design parameter. In this study, critical control margin chosen

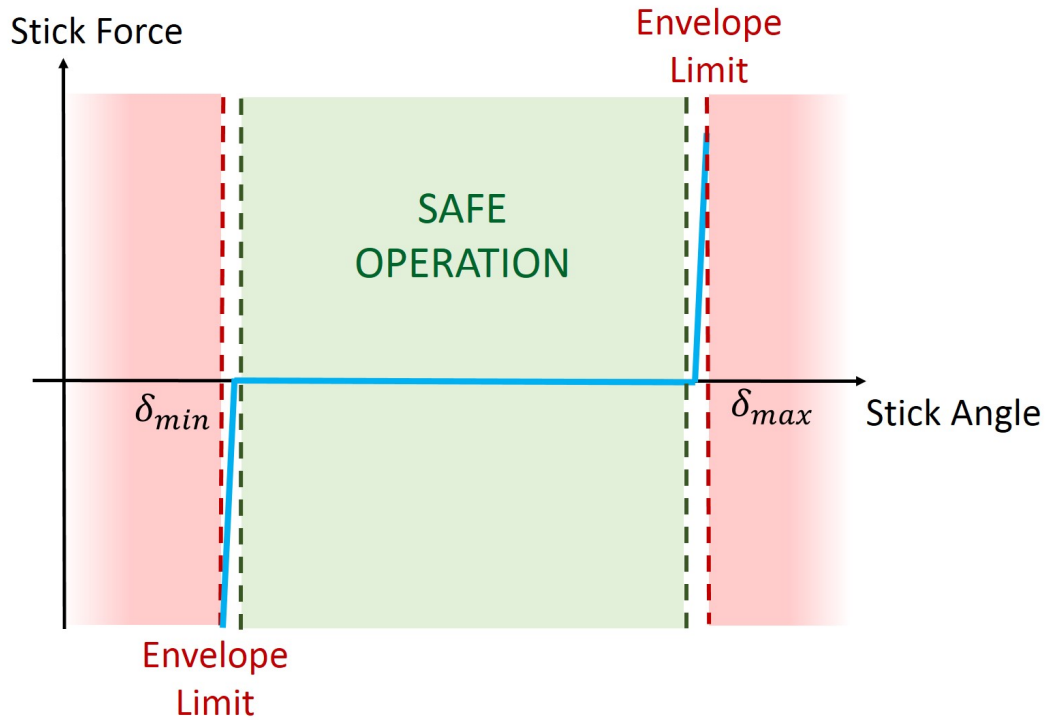


Figure 3.2: Hard Stop Force Profile

larger for faster inputs. This way limit avoidance algorithm acts more conservative during aggressive maneuvers where the risk of limit avoidance is greater. For slower inputs, a smaller critical margin is selected to increase the operational flight envelope. The stick angle at critical margin is fed to the inceptor as the greatest possible angle. This way moving the stick any further in the same direction is prevented. As the aircraft moves back to safe operation region the inceptor reverts back to its initial force profile.

3.2.2 Soft Stop Scheme

Soft stop force profile is illustrated in Fig. (3.3). Until the critical margin is reached, the stick acts similar to hard stop case. At the critical margin the force needed to move the stick increases. This prevents the pilot from exceeding the limit unwillingly. This approach gives the pilot authority to exceed the limit should they exert a greater force.

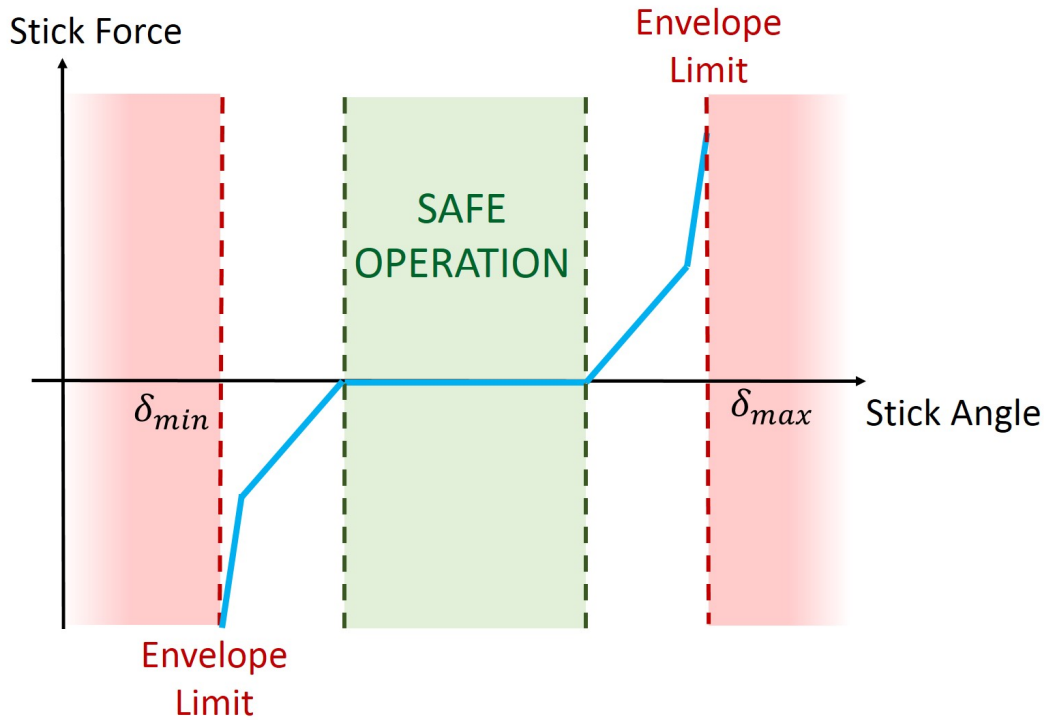


Figure 3.3: Soft Stop Force Profile

3.2.3 Force Gradient

Force gradient profile is illustrated in Fig. (3.4). In safe operation region the stick exerts little to no force, as control margin decreases stick force increases as a nonlinear function of control margin. The nonlinear relation between control margin, stick force and stick angle are given in Fig. (3.5). As control margin gets smaller, same force is applied at a smaller stick angle. This gradually increasing force warns the pilot that the vehicle is approaching to its limits. Moreover, the large force applied at envelope boundary prevent limit violation.

3.3 Application for a Rotorcraft

In this section implementation of the method given in chapter 2 to a rotorcraft model is explained in detail. The direct adaptive limit margin estimation method is applied to a high fidelity helicopter model consisting of a 3-state dynamic inflow model and

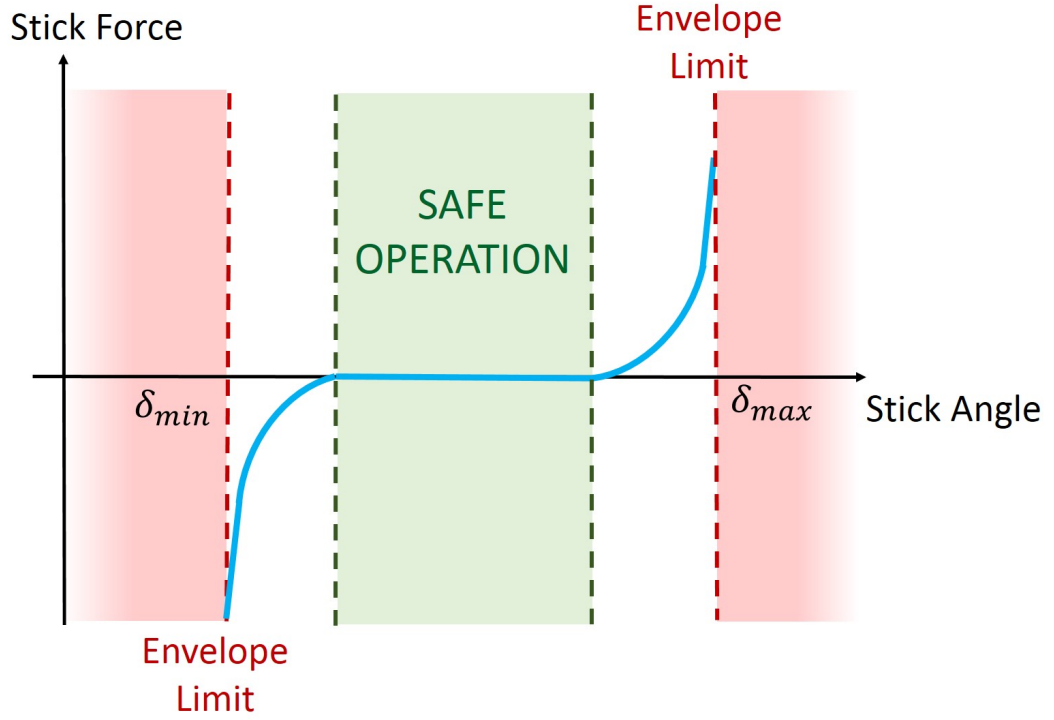


Figure 3.4: Force Gradient Profile

second order flapping dynamics in the main rotor given in [13]. The control margin estimation method is used to predict limits in longitudinal cyclic channel for load factor.

3.3.1 Problem Formulation

Fig.3.6 shows the simulation block diagram. An attitude stabilization system is used to help pilot to control the lateral dynamics and since the critical limit parameter is taken as the load factor, active controls are implemented on longitudinal channel. Dynamics of longitudinal states can be represented with following linear model:

$$\dot{\mathbf{x}} = A\mathbf{x} + B\mathbf{u} \quad (31)$$

where states are $\mathbf{x} = [u \ w \ q \ \theta]^T$ and the input is $u = \delta_{long}$. Fast states of the longitudinal dynamics are $\mathbf{x}_f = [w \ q]^T$ and slow states are $\mathbf{x}_s = [u \ \theta]^T$. For this

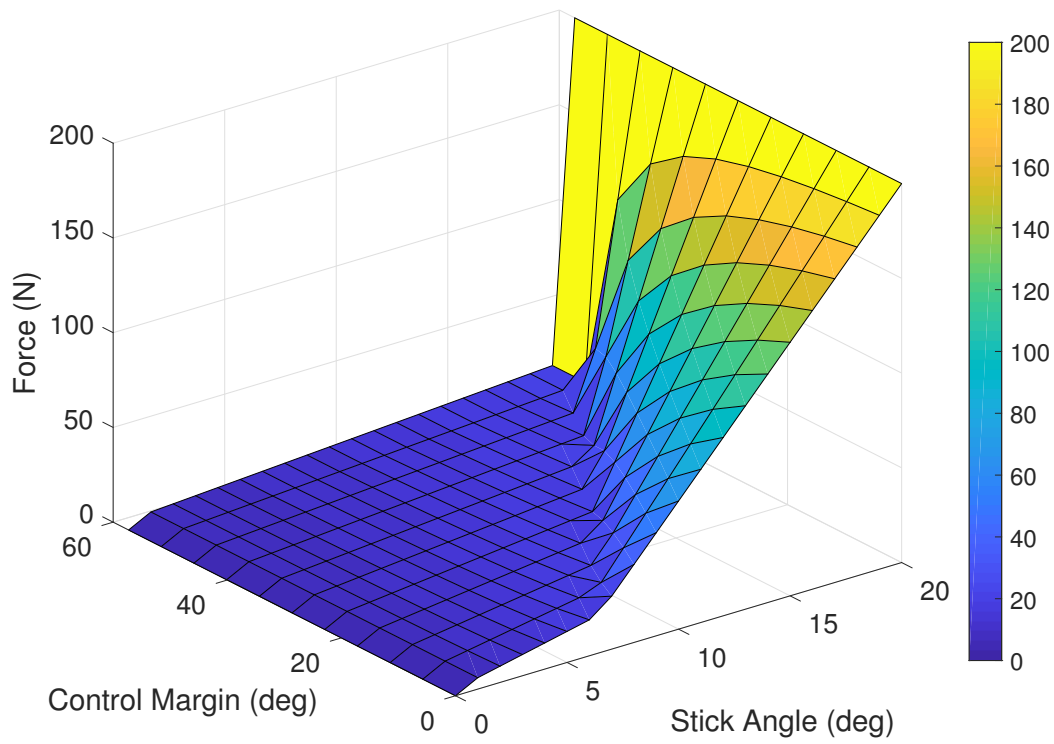


Figure 3.5: Force Map

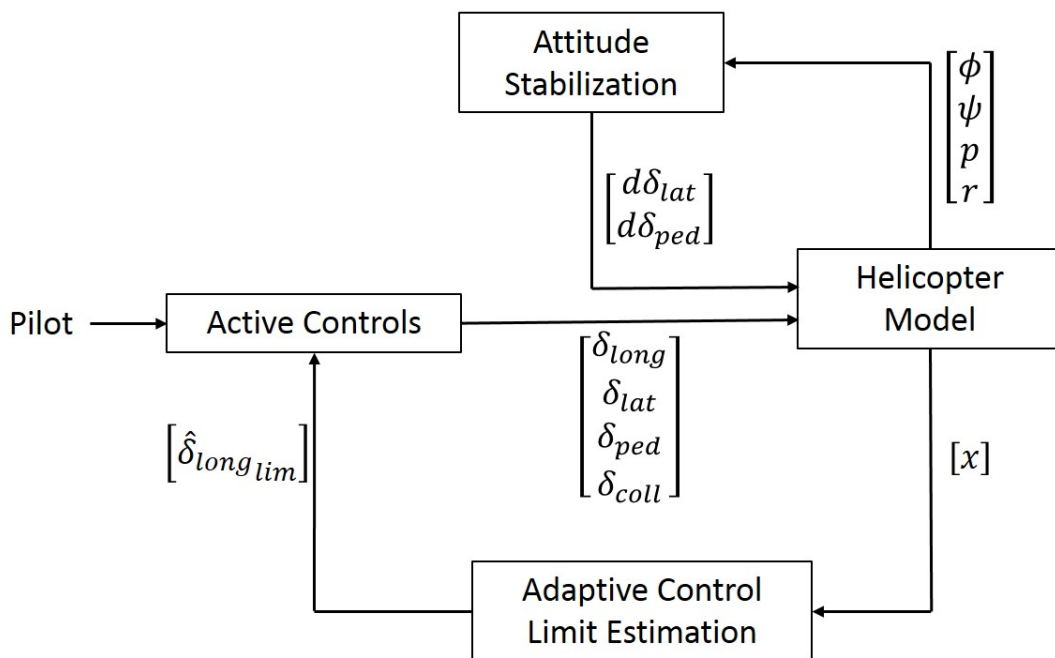


Figure 3.6: Simulation Block Diagram

problem Load factor is the critical envelope parameter and it is given by:

$$n_z = 1 + \frac{Vq}{g}. \quad (32)$$

where, V is the forward speed, q is the pitch rate and g is the gravitational acceleration. Load factor dynamics are dominated by pitch rate dynamics. Therefore, pitch rate model is constructed using the relation given in Eq. (219) at delayed time step as:

$$\begin{bmatrix} \hat{w} \\ \hat{q} \end{bmatrix}_d = -A_1^{-1} \left(- \begin{bmatrix} \dot{w} \\ \dot{q} \end{bmatrix} + A_2 \begin{bmatrix} u \\ \theta \end{bmatrix}_d + B_1 \delta_{long_d} \right) + \Delta(w, \dot{q}, u_d, \theta_d, \delta_{long_d}) \quad (33)$$

Inserting central difference terms into above equation:

$$\begin{bmatrix} \hat{w} \\ \hat{q} \end{bmatrix}_d = -A_1^{-1} \left(- \begin{bmatrix} \bar{\partial}(w)_d \\ \bar{\partial}(q)_d \end{bmatrix} + A_2 \begin{bmatrix} u \\ \theta \end{bmatrix}_d + B_1 \delta_{long_d} \right) + \Delta(\partial(w)_d, \partial(q)_d, u_d, \theta_d, \delta_{long_d}) \quad (34)$$

The dynamic trim value of pitch rate \hat{q}_{DT} , can be calculated by implementing Eq. (221) and inserting zero to derivative terms:

$$\begin{bmatrix} \hat{w} \\ \hat{q} \end{bmatrix}_{DT} = -A_1^{-1} \left(A_2 \begin{bmatrix} u \\ \theta \end{bmatrix}_d + B_1 \delta_{long_d} \right) + \Delta(0, 0, u_d, \theta_d, \delta_{long_d}) + e_d \quad (35)$$

where, the approximation error is $e_d = \begin{bmatrix} w \\ q \end{bmatrix}_d - \begin{bmatrix} \hat{w} \\ \hat{q} \end{bmatrix}_d$.

Dynamic trim value for load factor can be estimated using the relation in Eq.(32):

$$n_{zDT} = 1 + \frac{Vq_{DT}}{g} \quad (36)$$

Here, forward speed is a slow state; thus, it does not change much during dynamic trim. Then, the steady state limit margin becomes:

$$\hat{n}_{z_{marginDT}} = \hat{n}_{z_{lim}} - \hat{n}_{zDT}. \quad (37)$$

And, the limit margin based on the measured load factor is:

$$\hat{n}_{z_{margin}} = \hat{n}_{z_{lim}} - n_z. \quad (38)$$

The sensitivity of the pitch rate with respect to the longitudinal cyclic input, $S_q = \frac{\partial \hat{q}_{DT}}{\partial \delta_{long}}$, is

$$S_q = -A_1^{-1} B + \left[\frac{\partial \hat{q}_{DT}}{\partial \delta_{long}} \right]_{\dot{q}=0, \dot{w}=0} \quad (39)$$

The sensitivity of load factor with respect to elevator input is calculated using the relation in Eq. (36) and Eq. (39):

$$S_{n_z} = \frac{\partial \hat{n}_{zDT}}{\partial \delta_{long}} = \frac{-V}{g} S_q \quad (310)$$

Here, it is assumed that forward speed do not change much with respect to longitudinal cyclic input. Control sensitivity establishes a linear relationship between limit margin and control margin. Hence, using Eq.(227) , the control limits become:

$$\hat{\delta}_{long_{lim-upper}} = \min \left(\left| \frac{1}{S} \hat{n}_{z_{margin}} \right|, \left| \frac{1}{S} \hat{n}_{z_{marginDT}} \right| \right) + \delta_{long} \quad (311)$$

$$\hat{\delta}_{long_{lim-lower}} = -\min \left(\left| \frac{1}{S} \hat{n}_{z_{margin}} \right|, \left| \frac{1}{S} \hat{n}_{z_{marginDT}} \right| \right) + \delta_{long} \quad (312)$$

where, $\hat{n}_{z_{marginDT}}$ is the steady state limit margin and $\hat{n}_{z_{margin}}$ is the limit margin based on measured load factor.

3.3.2 Adaptive Neural Network Augmentation with SHL Concurrent Learning

The learning algorithm for the adaptive element introduced in Eq. (326) is selected as Concurrent Learning, which is an adaptive learning scheme that uses recorded data for learning and does not require persistency of excitation [5]. Concurrent learning is used with both linear parameter neural network (LPNN) and single hidden layer neural network (SHL NN) structures in this work.

For structured uncertainties that are linearly parametrizable LPNN scheme can be used. Although the aircraft model is nonlinear and the structure of the uncertainty is not exactly known, when LPNN scheme is used weights will be bounded around the optimal weights [8]. For LPNN the adaptive element Δ can be constructed as:

$$\Delta(\bar{x}) = \mathbf{W}^T \Phi(\bar{x}). \quad (313)$$

where, the basis vector \bar{x} is selected as:

$$\Phi(i) = \phi_i(\partial(q)_d(i)), \quad i = 1 : 4 \quad (314)$$

$$\Phi(i + 4) = \phi_{i+4}(\partial(w)_d(i)), \quad i = 1 : 4 \quad (315)$$

$$\Phi(9 : 15) = [\phi_9(u) \ \phi_{10}(\theta) \ \phi_{11}(\delta_{long}) \ \phi_{12}(\delta_{long}u) \ \phi_{13}(\delta_{long}\theta) \ \phi_{14}(u\theta) \ b_1]^T \quad (316)$$

The activation function $\phi_i(\cdot)$ is selected as hyperbolic tangent function to ensure boundedness:

$$\phi_i(\cdot) = a_i \tanh\left(\frac{\cdot}{a_i}\right) \quad i = 1, 2, \dots, 15 \quad (317)$$

The a_i in Eq. (345) are design parameters.

Single Hidden Layer Neural Network (SHL NN) scheme is often used for continuous unstructured uncertainties. In this case exact knowledge of the uncertainty is not required. The uncertainty Δ can be constructed with SHL NN as:

$$\Delta(\bar{\mathbf{x}}) = \mathbf{W}^T \boldsymbol{\sigma}(\mathbf{V}^T \bar{\mathbf{x}}) \quad (318)$$

For this problem number of single hidden layer neurons is selected as 3. Then, the synaptic weight matrix between hidden layer and output layer becomes:

$$\mathbf{W} = \begin{bmatrix} \theta_w \\ w_1 \\ w_2 \\ w_3 \end{bmatrix} \in \Re^{4 \times 1} \quad (319)$$

Here, θ_w is the bias and w_i are synaptic weights. Similarly, the synaptic weight matrix between input layer and hidden layer is:

$$\mathbf{V} = \begin{bmatrix} \theta_{v,1} & \theta_{v,2} & \theta_{v,3} \\ v_{1,1} & v_{1,2} & v_{1,3} \\ \vdots & \vdots & \vdots \\ v_{12,1} & v_{12,2} & v_{12,3} \end{bmatrix} \in \Re^{13 \times 3} \quad (320)$$

Here, $\theta_{v,i}$ are bias and $v_{i,j}$ are synaptic weights. The input vector of SHL NN, $\bar{\mathbf{x}}$ is:

$$\bar{\mathbf{x}} = \begin{bmatrix} b_v \\ x_{in} \end{bmatrix} = \begin{bmatrix} b_v \\ \partial(q)_{1_d} \\ \vdots \\ \partial(q)_{4_d} \\ \partial(w)_{1_d} \\ \vdots \\ \partial(w)_{4_d} \\ u_d \\ \theta_d \\ \delta_{long_d} \end{bmatrix} \in \Re^{12 \times 1} \quad (321)$$

Finally, the sigmoidal activation functions are in the form:

$$\boldsymbol{\sigma}(\mathbf{z}) = \begin{bmatrix} b_w \\ \sigma_1(z_1) \\ \sigma_2(z_2) \\ \sigma_3(z_3) \end{bmatrix} \in \mathfrak{R}^{4 \times 1} \quad (322)$$

where, $\mathbf{z} = \mathbf{V}^T \bar{\mathbf{x}}$ and elements of $\boldsymbol{\sigma}$ are:

$$\sigma_i(z_i) = \frac{1}{1 + e^{-a_i z_i}} \quad (323)$$

with a_i 's as design parameters.

3.3.3 Simulation Results for Helicopter Load Factor Protection

In this section simulation results for example cases are presented. For simulations a high fidelity helicopter model consisting of a 3-state dynamic inflow model and second order flapping dynamics in the main rotor is used [13] and load factor output of a helicopter model is considered as the critical limit parameter. Upper limit for load factor is assumed to be 3. Time step of the simulations are 30 Hz and the solver uses Euler's Method. Example cases include forward flight at different speeds, climb, and descent at constant rate. In each case the helicopter is given longitudinal cyclic inputs to perform pull-up/push-over maneuvers. During simulations an attitude stabilization system is employed to help pilot to control the lateral dynamics and the longitudinal channel is made open loop.

3.3.3.1 Case 1 : Adaptive Control Limit Estimation

The first case demonstrates the online modeling capability of the control limit estimation algorithm using both LPNN and SHL NN for concurrent learning. For this case, helicopter model is trimmed at 1000 ft attitude and 100 kt forward speed. For

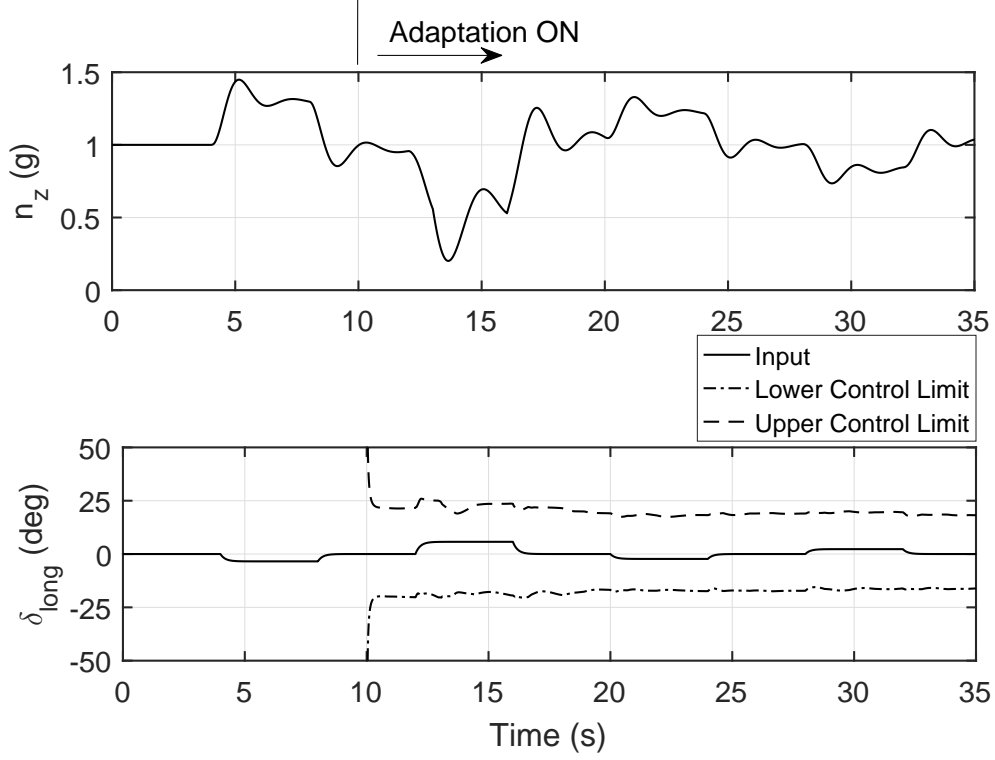


Figure 3.7: Load Factor and Control Margins, Case-1, LPNN

this flight condition following approximate linear model is generated:

$$\begin{bmatrix} \dot{u} \\ \dot{w} \\ \dot{q} \\ \dot{\theta} \end{bmatrix} = \begin{bmatrix} -0.3 & 0.20 & 17.05 & -31.97 \\ 0.14 & -1.17 & 179.87 & 3.24 \\ 0.005 & -0.045 & -0.52 & 0 \\ 0 & 0 & 1 & 0 \end{bmatrix} \begin{bmatrix} u \\ w \\ q \\ \theta \end{bmatrix} + \begin{bmatrix} 0.37 \\ 174.61 \\ -0.95 \\ -0.009 \end{bmatrix} \delta_{long} \quad (324)$$

First, results for LPNN CL are presented. In Fig. (3.16) load factor and longitudinal cyclic input with online estimated control limits are plotted. The adaptive limit margin estimation method is OFF in first 10 seconds and it is turned ON at $t = 10s$. When the adaptation is turned ON, the control limit estimation converges to its steady values. In Fig. (3.8) model error and singular value of the history stack are plotted. As it can be seen from the figure, adaptive element fully compensates for the model error after the adaptation is turned ON. The recording algorithm of concurrent learning employs the singular value maximization approach. Fig. (3.8) demonstrates that singular value of the history stack keeps increasing; thus, relevant data is recorded properly. Helicopter states for this maneuver is presented in Fig. (3.9). The attitude

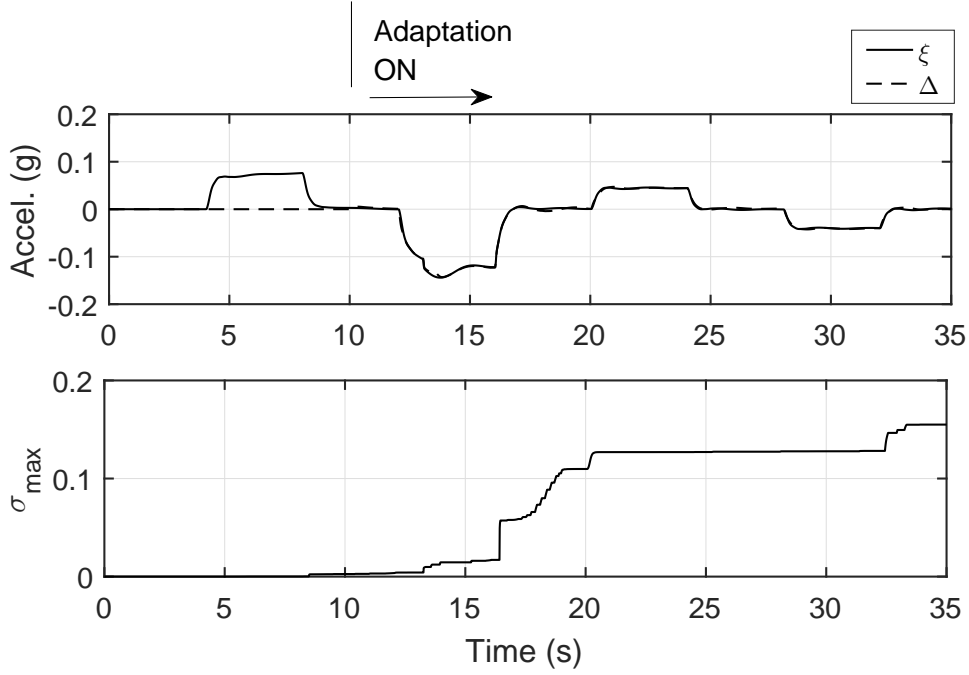


Figure 3.8: Model Error and Singular Value, Case-1, LPNN

stabilization system keeps the lateral states around the trim condition. Adaptive weights for LPNN CL and control sensitivity are shown in Fig. (3.10). After the adaptation is ON, the control sensitivity oscillates around its steady-optimal value. In Fig. (3.11) performance of the control limit estimation method through an aggressive maneuver where envelope limits are violated is shown. Note that, the envelope limits are violated when the control input exceeds the control limits. This case is also solved with SHL NN CL as the adaptive element. In Fig. (3.12) load factor and longitudinal cyclic input with online estimated control limits are plotted. The adaptive limit margin estimation method is OFF in first 10 seconds and it is turned ON at $t = 10s$. When the adaptation is turned ON, the control limit estimation converges to its steady values. In Fig. (3.13) model error and singular value of the history stack are plotted. As it can be seen from the figure, adaptive element fully compensates for the model error after the adaptation is turned ON. Since this is a simple case there is no performance difference between LPNN and SHL NN are observed. Fig. (3.13) also demonstrates that singular value of the history stack is increasing. Adaptive

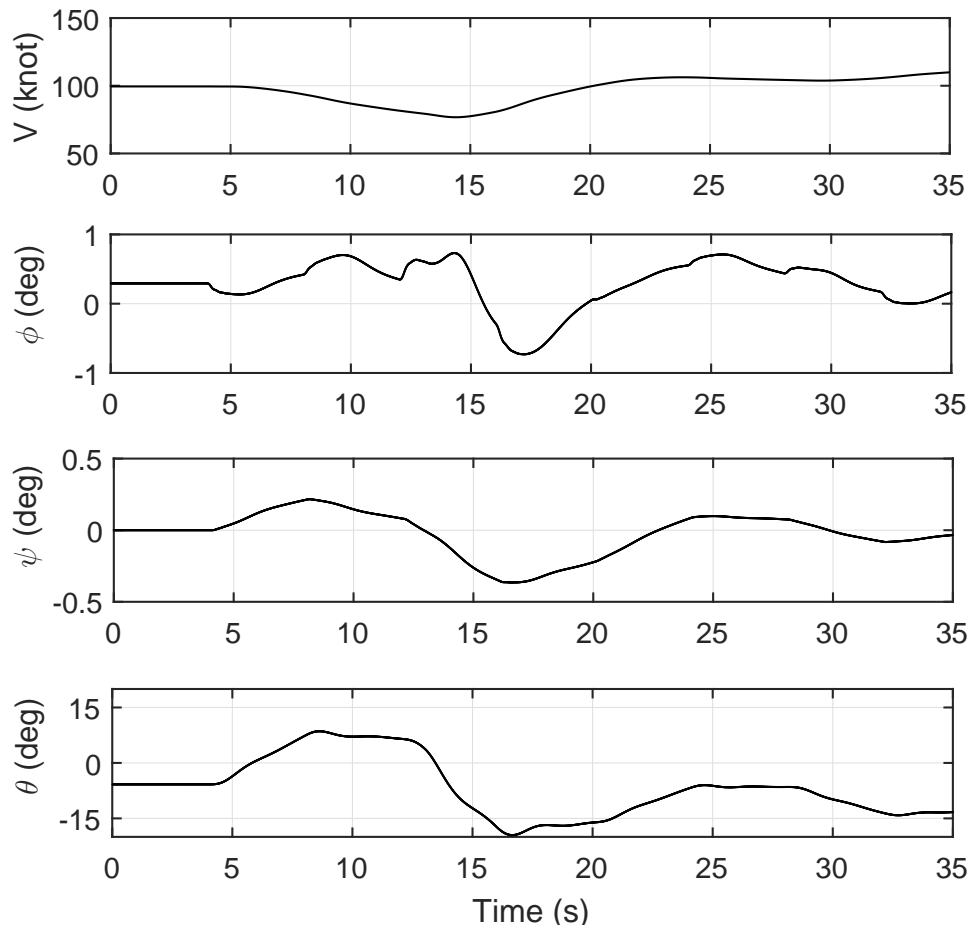


Figure 3.9: Helicopter States, Case-1, LPNN

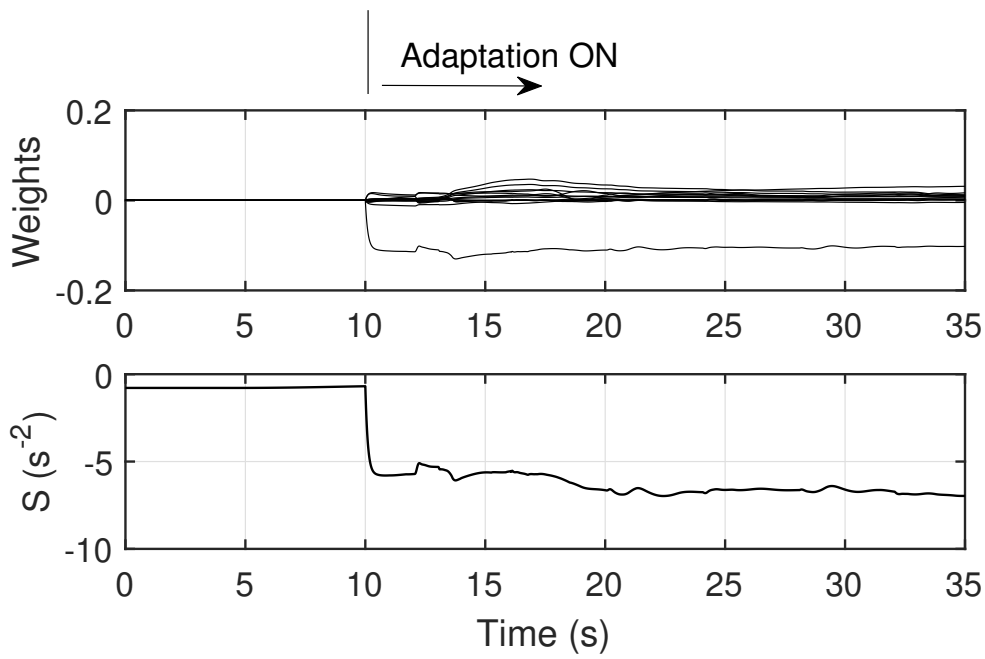


Figure 3.10: Weights and Sensitivity, Case-1, LPNN

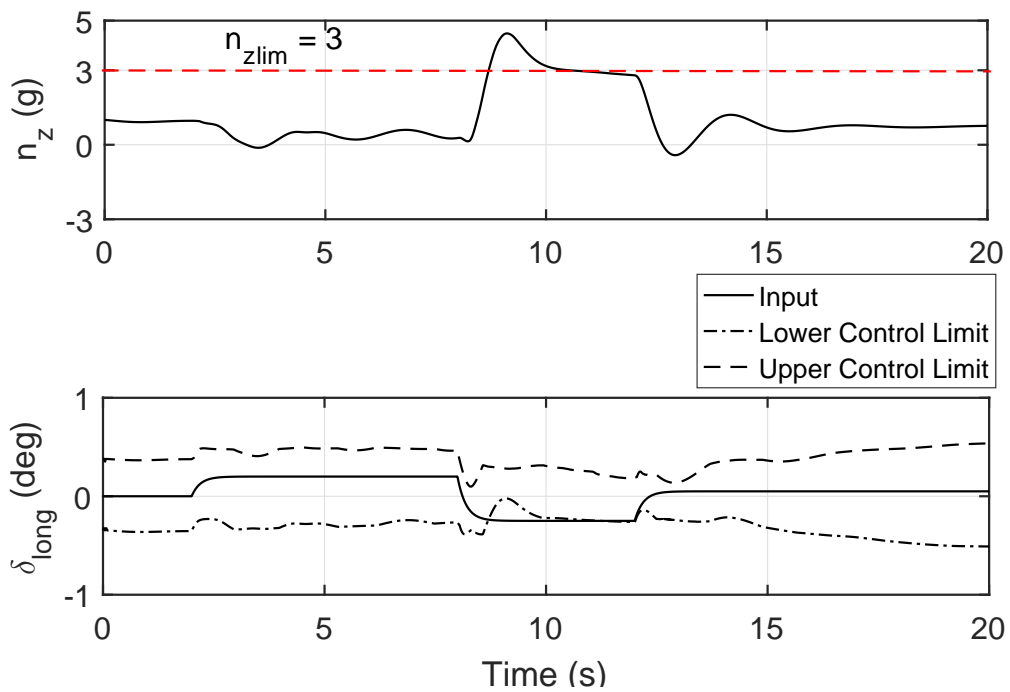


Figure 3.11: Aggressive Input, Case-1, LPNN

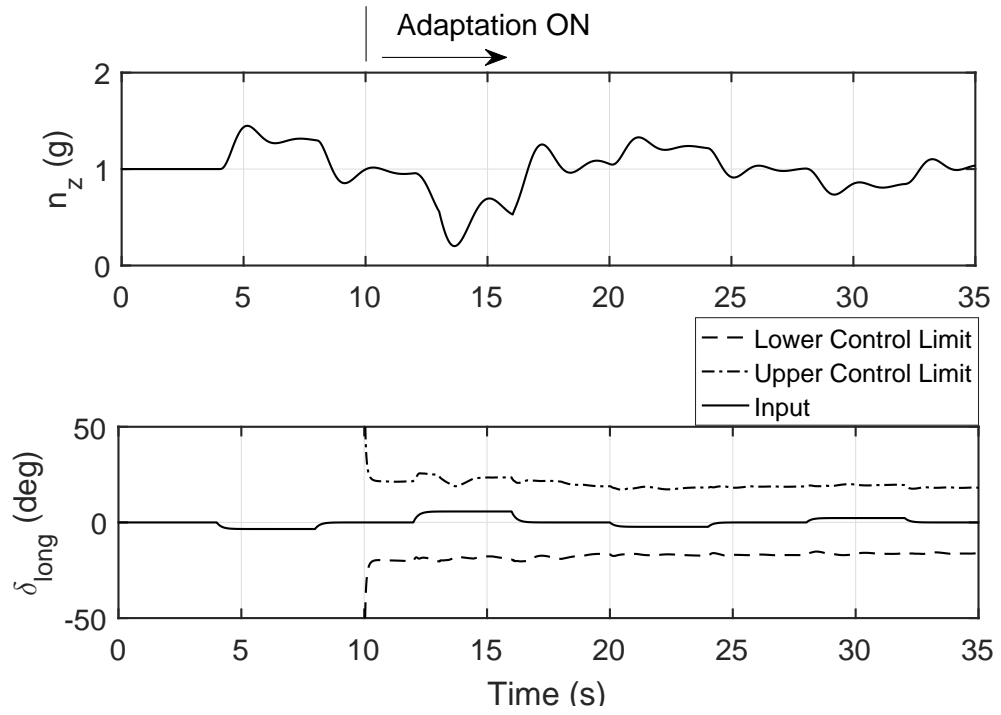


Figure 3.12: Load Factor and Control Margins, Case-1, SHL NN

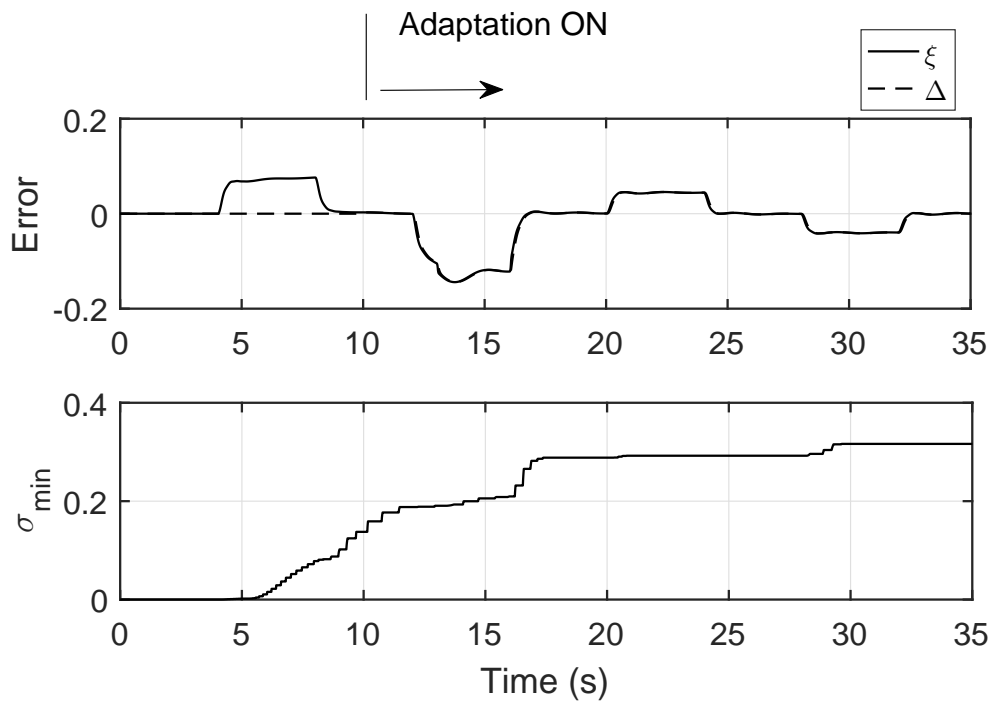


Figure 3.13: Model Error and Singular Value, SHL NN, Case-1

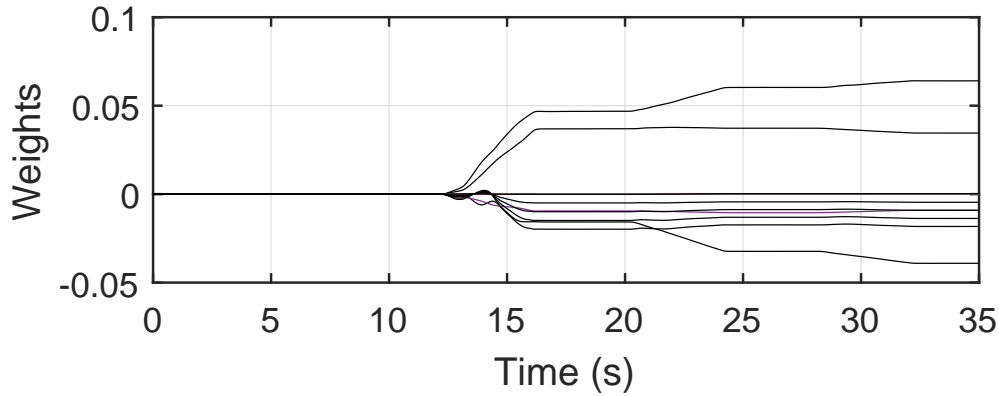


Figure 3.14: Weights, SHL NN, Case-1

weights that connect the input layer to hidden layer for SHL NN CL are shown in Fig. (3.14). After the adaptation is ON, the weights are convergent. In Fig. (3.15) performance of the control limit estimation method through an aggressive maneuver where envelope limits are violated is shown. Note that, the envelope limits are violated when the control input exceeds the control limits.

3.3.3.2 Case-2 : Limit Avoidance with Active Side Stick

For this case, real time simulations are run on simulator test bench described in section 3.2 and the active side stick introduced in section 3.2 is used for producing the longitudinal cyclic input. The active side stick gives force feedback cues to the pilot to prevent limit violation. The force profile given in Fig. (3.5) is employed. Aggressive inputs that can violate the envelope limits are given to the helicopter in order to test the limit avoidance capabilities of the active side stick. For this case both LPNN CL and SHL NN CL are considered as adaptive element. The linear model given in Eq. (324) is used for all simulations.

First, simulation results with LPNN CL are presented. For this simulation the helicopter is trimmed at 1000 ft attitude and 100 kt forward speed. First, with a push over input the helicopter gains some speed. Then, the pilot slowly pulls up to increase load factor. The active side stick stiffens as control margin gets smaller. Then, same maneuver is repeated with a more aggressive pull up input. Longitudinal cyclic input and load factor response is plotted in Fig. (3.16). Note that, for both pull ups limit

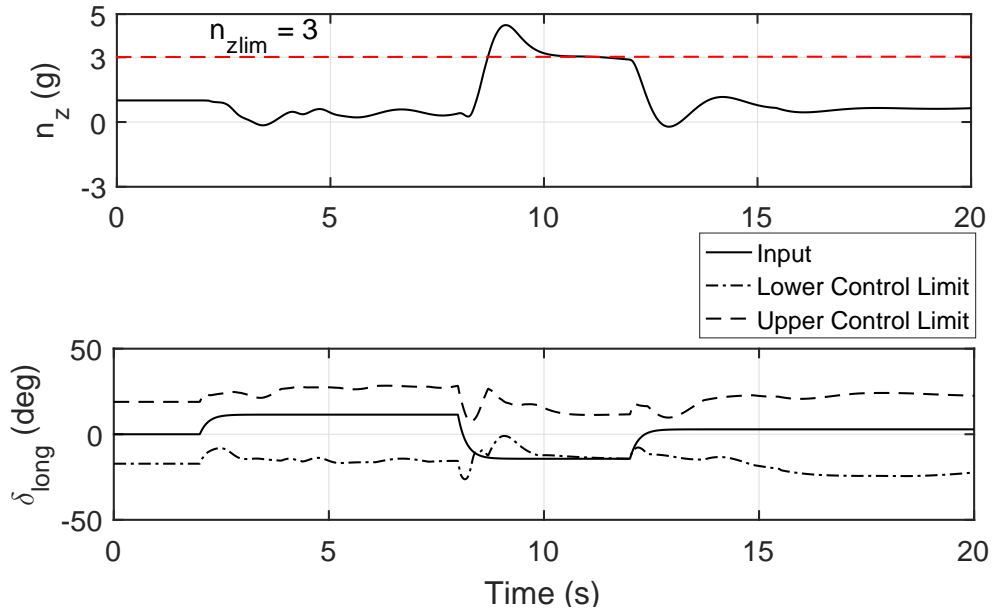


Figure 3.15: Aggressive Input, SHL NN, Case-1

violation is avoided. The force on the active side stick is plotted in Fig. (3.17). As control margin decreases, stick force increases. Moreover, with a stiffer increase at the control limit, envelope limit violation is prevented. Model error compensation and minimum singular value of the history stack are plotted in Fig. (3.18). Small errors in model error compensation are reasonable. A similar maneuver at the same flight conditions is also performed with SHL NN CL as the adaptive element. After accelerating the helicopter pilot performs one slow and one aggressive pull up maneuver. In Fig. (3.19) load factor response and control input with estimated control limits are plotted. Limit violation is prevented due to the force feedback exerted by the active side stick. Stick force is plotted in Fig. (3.20). The force on the stick is smaller for slow pull up maneuver; whereas, for the aggressive pull up stick also responds aggressively with greater force feedback. Model error and minimum singular value are plotted in Fig. (3.21). Better performance of SHL NN scheme can be observed here.

Finally, in order to see the effectiveness of the control limit predictions for different flight conditions simulations are repeated at a different air speed and for different climb rates. For these simulations the neural network is trained at 100 kt forward

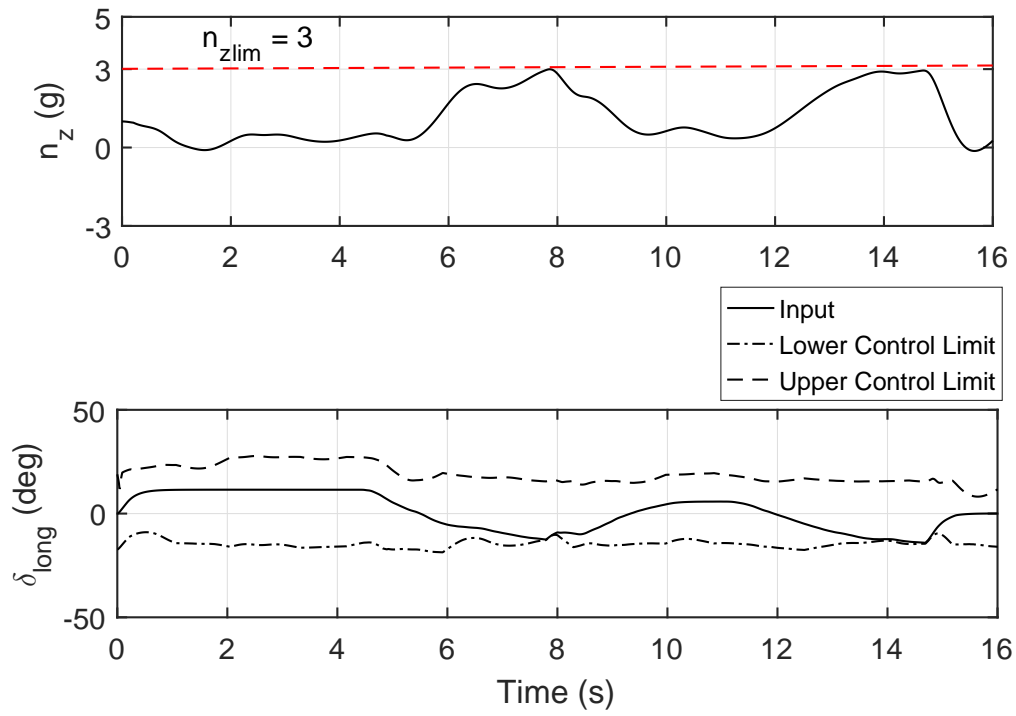


Figure 3.16: Load Factor and Control Margins, Case-2, LPNN

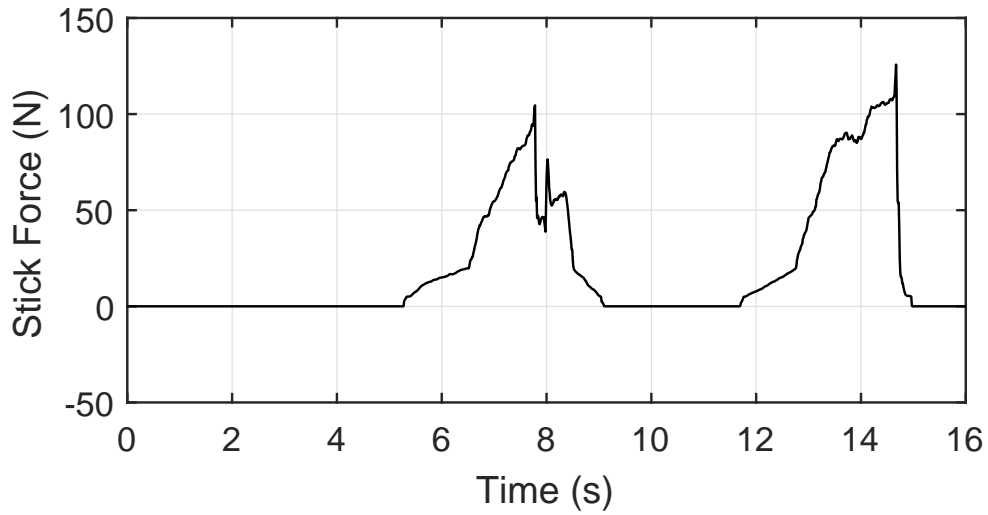


Figure 3.17: Stick Force, Case-2, LPNN

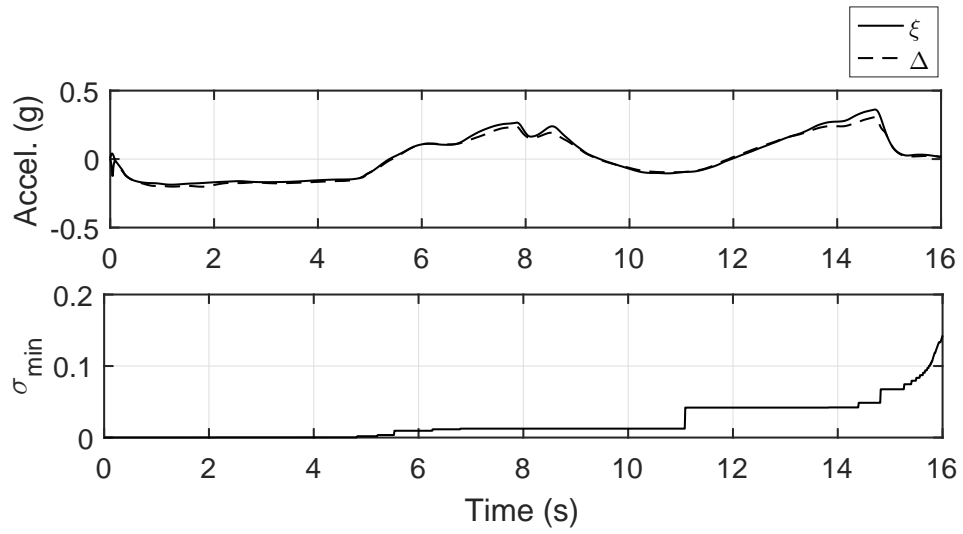


Figure 3.18: Model Error and Singular Value, Case-2, LPNN

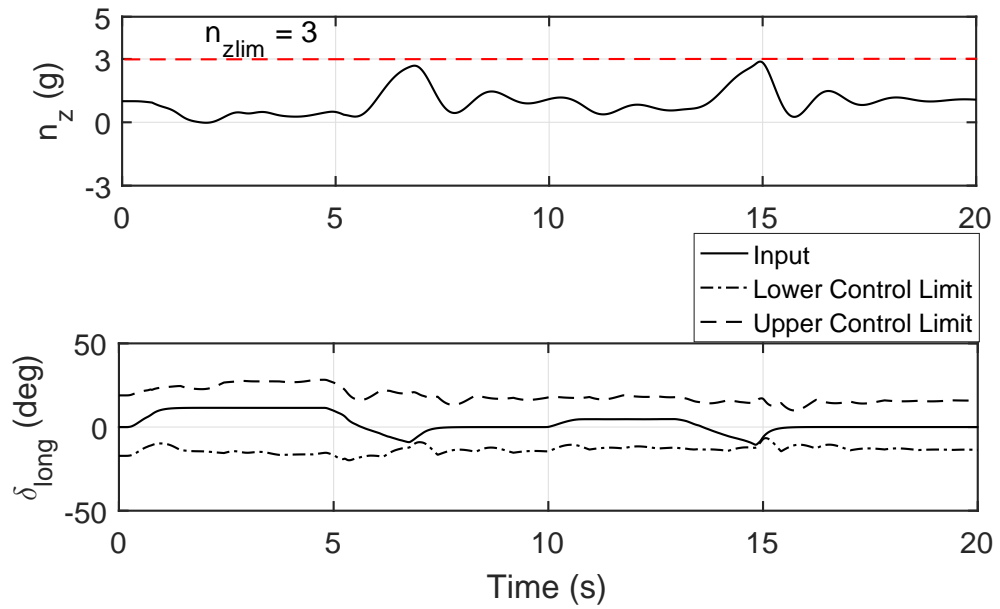


Figure 3.19: Load Factor and Control Margins, Case-2, SHL NN

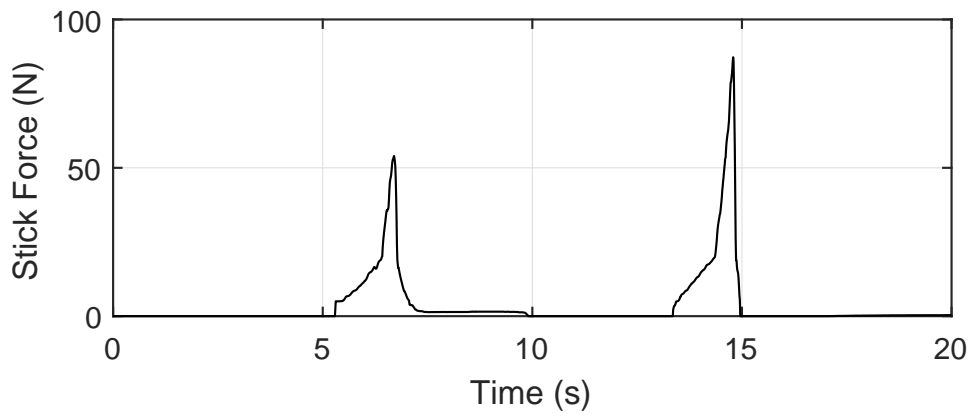


Figure 3.20: Stick Force, Case-2, SHL NN

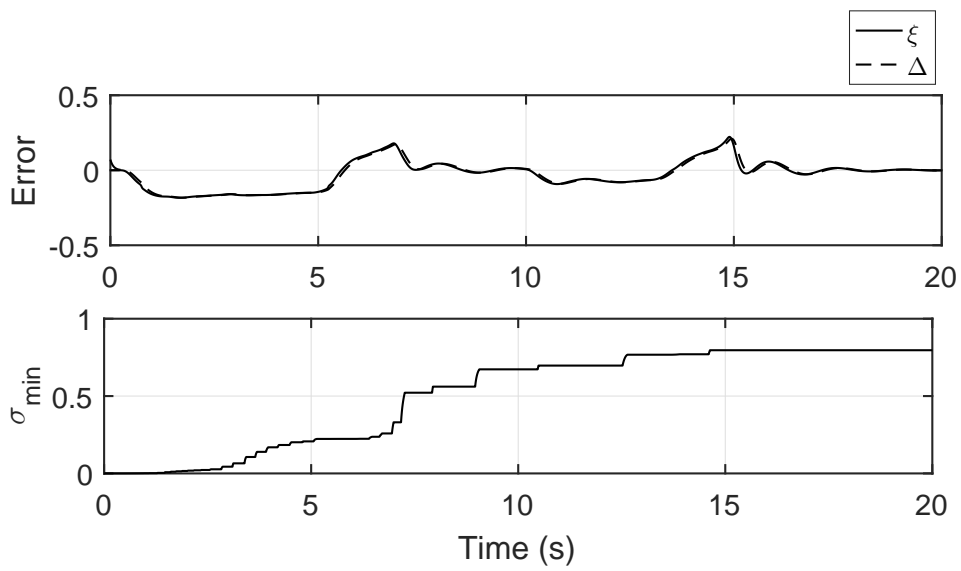


Figure 3.21: Model Error and Singular Value, Case-2, SHL NN

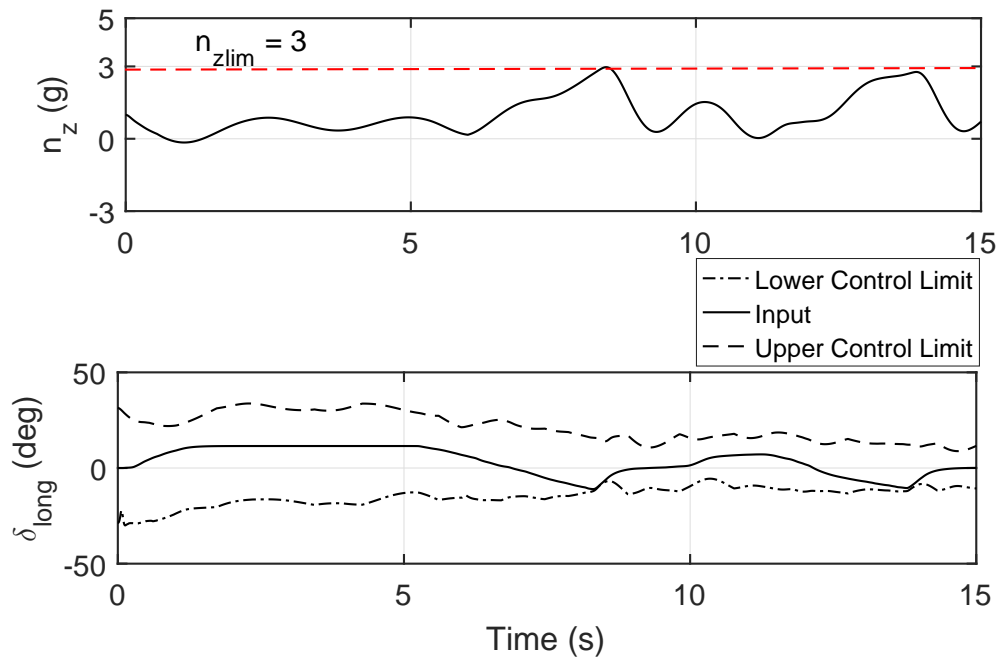


Figure 3.22: Load Factor and Control Margins for 60 kt Forward Flight

speed. In Fig. (3.22) load factor response and control input for 60 kt forward flight is presented. Model error plot for the corresponding flight condition is given in Fig. (3.23). Increase in error in compensation is caused by deviation from initial linear approximate model and inability of the neural network to unlearn its previous training. The performance can be improved by introducing purging algorithms. In Fig. (3.24) load factor response and control input for 1734 fpm climb at 60 kt is presented. Model error plot for the corresponding flight condition is given in Fig. (3.25). In Fig. (3.26) load factor response and control input for 1350 fpm descend at 60 kt is presented. Model error plot for the corresponding flight condition is given in Fig. (3.27). Worst performance is observed for this flight condition.

3.4 Application for a Fixed Wing Aircraft

In this section the method given in chapter 2 is applied to a fixed wing aircraft model given in [19]. The control margin estimation method is used to predict limits in elevator channel for both angle of attack and load factor.

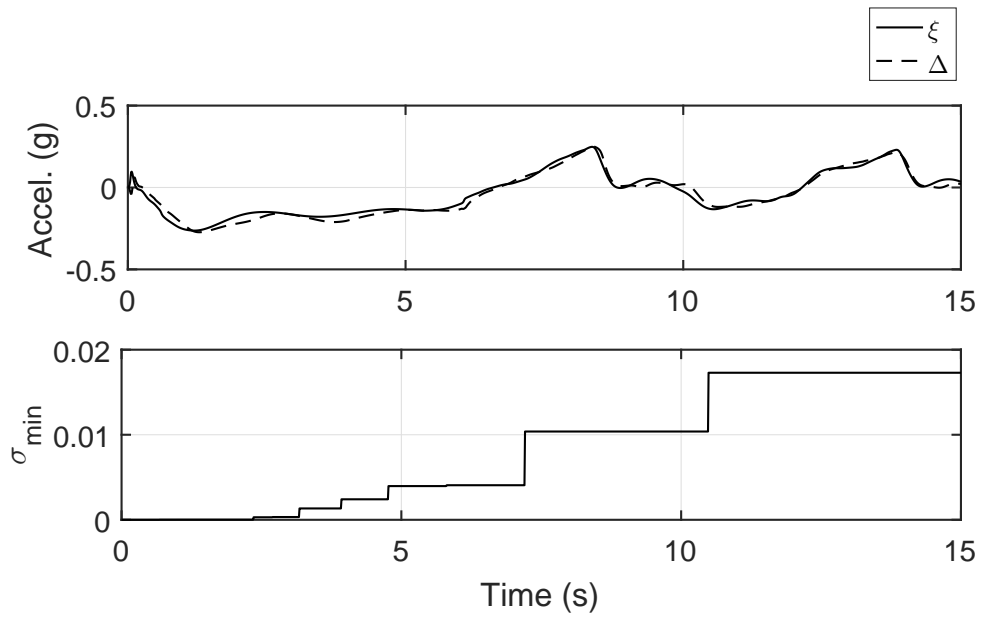


Figure 3.23: Model Error and Singular Value for 60 kt Forward Flight

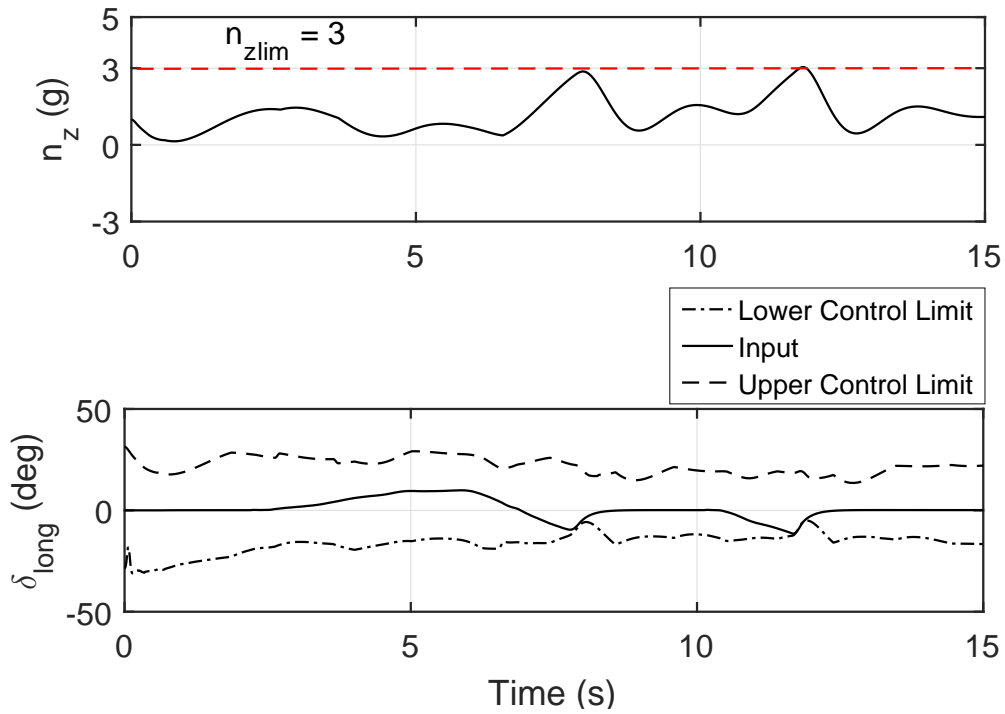


Figure 3.24: Load Factor and Control Margins for 1734 fpm Climb

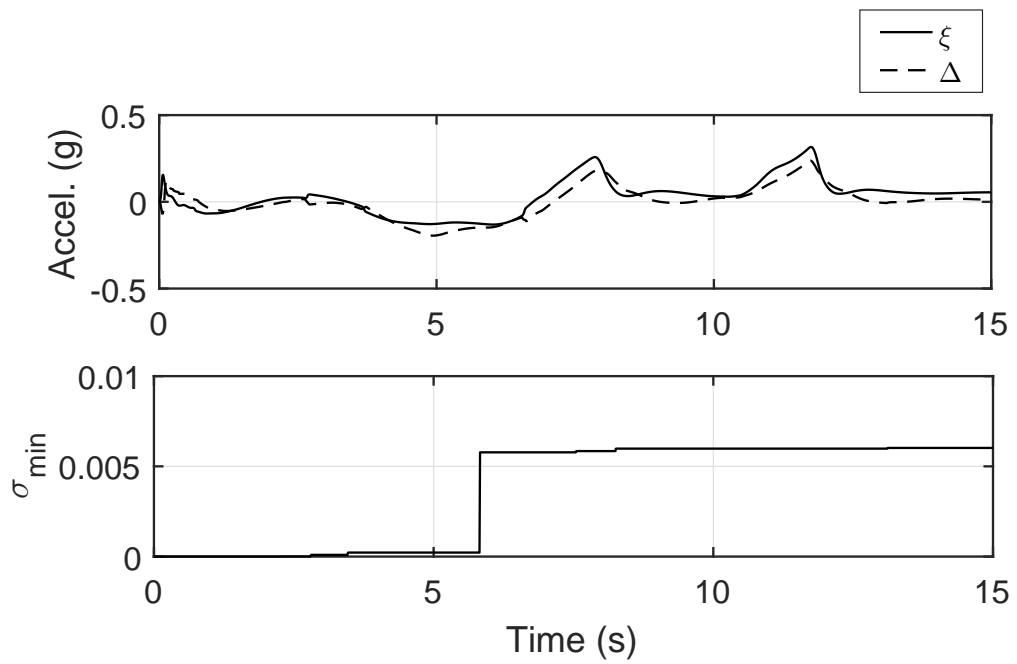


Figure 3.25: Model Error and Singular Value for 1734 fpm Climb

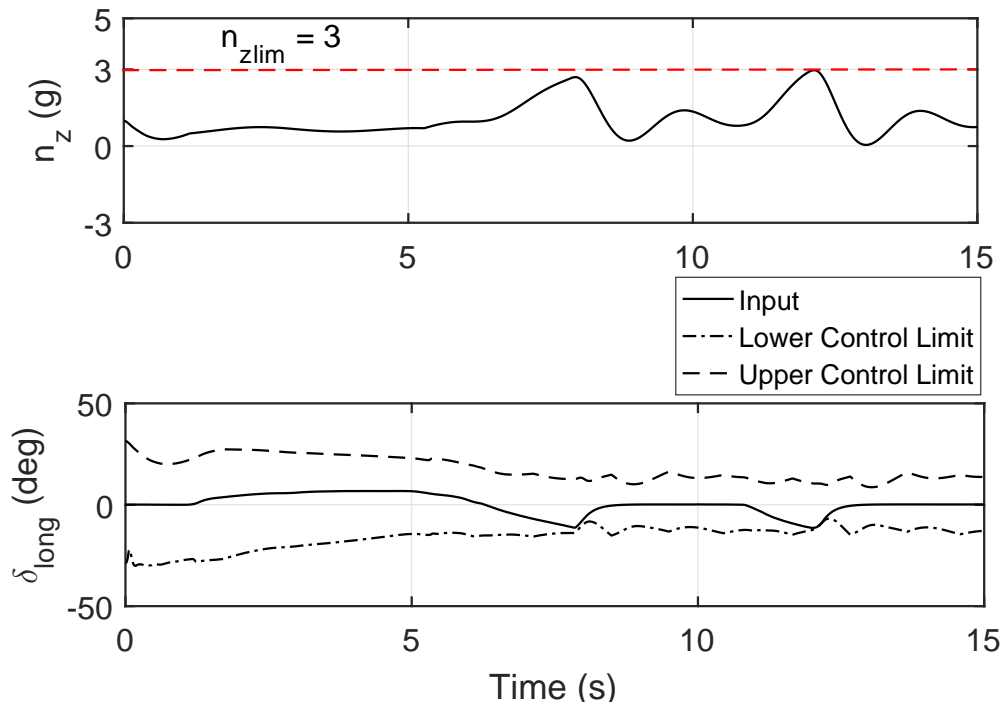


Figure 3.26: Load Factor and Control Margins for 1350 fpm Descend

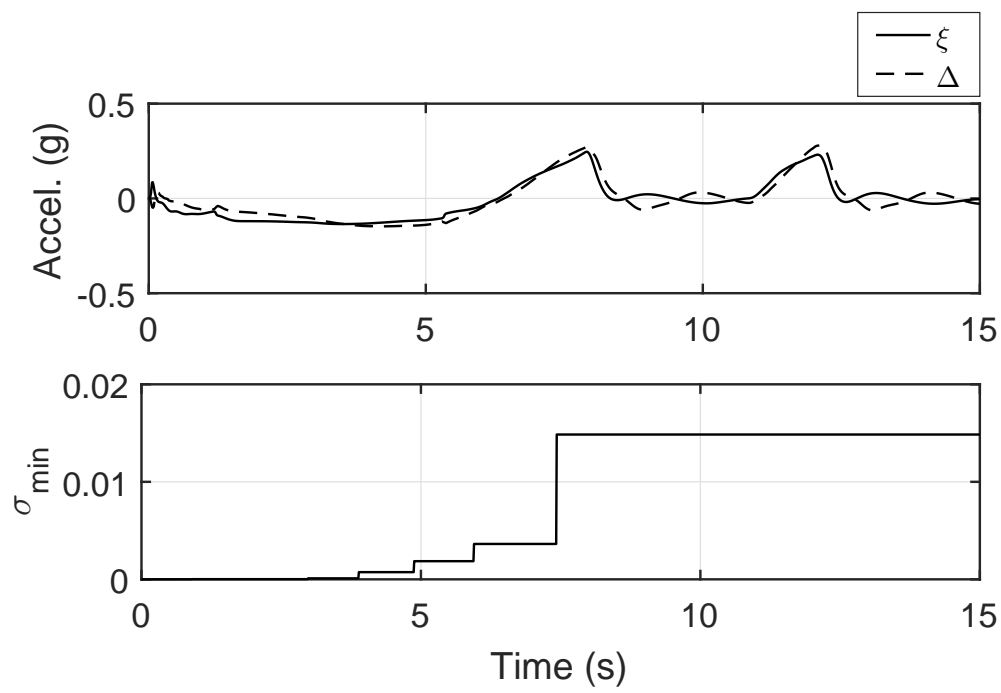


Figure 3.27: Model Error and Singular Value for 1350 fpm Descend

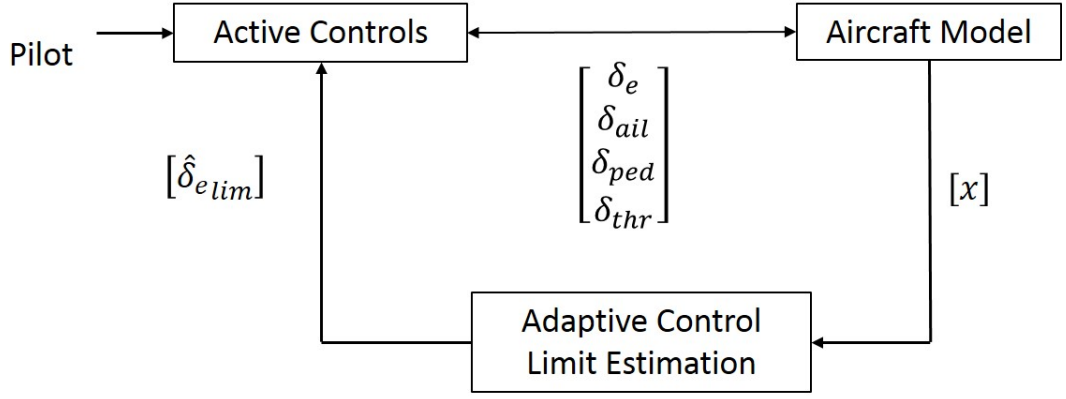


Figure 3.28: Simulation Block Diagram

3.4.1 Problem Formulation

For this section consider the simulation block diagram in Fig.3.28, where both the longitudinal channel and the lateral channel are made open loop. The pilot can control the lateral dynamics through pedals and active side stick and longitudinal dynamics through throttle and active side stick. The active side stick is used for controlling both pitch movement and roll movement; however, only the longitudinal channel is programmed for envelope protection. In this setup load factor and angle of attack are considered as the critical parameters and the control margins for elevator input are estimated online following [10] and [18]. Dynamics of longitudinal states can be represented with following linear model:

$$\dot{\mathbf{x}} = A\mathbf{x} + B\mathbf{u} \quad (325)$$

where states are $\mathbf{x} = [V \ \alpha \ q \ \theta]^T$ and the input is $u = \delta_e$. Fast states of the longitudinal dynamics are $\mathbf{x}_f = [\alpha \ q]^T$ and slow states are $\mathbf{x}_s = [V \ \theta]^T$. Then, using the relation given in Eq. (219) fast states α and q can be estimated at delayed time step as:

$$\begin{bmatrix} \hat{\alpha} \\ \hat{q} \end{bmatrix}_d = -A_1^{-1} \left(- \begin{bmatrix} \dot{\alpha} \\ \dot{q} \end{bmatrix} + A_2 \begin{bmatrix} V \\ \theta \end{bmatrix}_d + B_1 \delta_{e_d} \right) + \Delta(\dot{\alpha}, \dot{q}, V_d, \theta_d, \delta_{e_d}) \quad (326)$$

Inserting central difference terms into above equation we get the fast state estimate as:

$$\begin{bmatrix} \hat{\alpha} \\ \hat{q} \end{bmatrix}_d = -A_1^{-1} \left(- \begin{bmatrix} \bar{\partial}(\alpha)_d \\ \bar{\partial}(q)_d \end{bmatrix} + A_2 \begin{bmatrix} V \\ \theta \end{bmatrix}_d + B_1 \delta_{e_d} \right) + \Delta(\partial(\alpha)_d, \partial(q)_d, V_d, \theta_d, \delta_{e_d}) \quad (327)$$

The dynamic trim value of fast states, $\hat{\alpha}_{DT}$ and \hat{q}_{DT} , can be calculated by implementing Eq. (221) and inserting zero to derivative terms:

$$\begin{bmatrix} \hat{\alpha} \\ \hat{q} \end{bmatrix}_{DT} = -A_1^{-1} \left(A_2 \begin{bmatrix} V \\ \theta \end{bmatrix}_d + B_1 \delta_{e_d} \right) + \Delta(0, 0, V_d, \theta_d, \delta_{e_d}) + e_d \quad (328)$$

where, the approximation error is $e_d = \begin{bmatrix} \alpha \\ q \end{bmatrix}_d - \begin{bmatrix} \hat{\alpha} \\ \hat{q} \end{bmatrix}_d$.

3.4.1.1 Load Factor as the Critical Limit Parameter

Load factor for a fixed wing aircraft is given by [19]:

$$n_z = \frac{1}{g}(\dot{w} + vp - uq) + \cos \theta \cos \phi \quad (329)$$

Here, u , v , and w are components of aircraft's velocity written in body fixed reference frame. p and ϕ are roll rate and roll angle respectively. Similarly, q and θ are pitch rate and pitch angle respectively. g is the gravitational acceleration. Load factor response is dominated by pitch rate (q). Therefore, a model of the pitch rate is generated and load factor is calculated later using Eq.(329). Dynamic trim value for load factor can be estimated as:

$$n_{z_{DT}} = \frac{1}{g}(vp - uq_{DT}) + \cos \theta \cos \phi \quad (330)$$

Here, Euler angles and velocities are slow states; thus, they do not change much during dynamic trim. Roll rate, p is also assumed to be changing slowly with elevator inputs. Then, the steady state limit margin becomes:

$$\hat{n}_{z_{marg_{DT}}} = \hat{n}_{z_{lim}} - \hat{n}_{z_{DT}}. \quad (331)$$

And, the limit margin based on the measured load factor is:

$$\hat{n}_{z_{marg}} = \hat{n}_{z_{lim}} - n_z. \quad (332)$$

The sensitivity of the pitch rate with respect to the elevator input, $S_q = \frac{\partial \hat{q}_{DT}}{\partial \delta_e}$, is

$$S_q = -A_1^{-1}B + \left[\frac{\partial \hat{q}_{DT}}{\partial \delta_e} \right]_{\dot{q}=0, \dot{\alpha}=0} \quad (333)$$

The sensitivity of load factor with respect to elevator input is calculated using the relation in Eq. (330) and Eq. (333):

$$S_{n_z} = \frac{\partial \hat{n}_{zDT}}{\partial \delta_e} \quad (334)$$

$$S_{n_z} = \frac{-u}{g} S_q \quad (335)$$

Here, it is assumed that slow states and lateral states do not change much with respect to elevator input. Control sensitivity establishes a linear relationship between limit margin and control margin. Hence, using Eq.(227) , the control limits become:

$$\delta_{e_{lim}} = \min \left(\left| \frac{1}{S_{n_z}} \hat{n}_{z_{margin}} \right|, \left| \frac{1}{S_{n_z}} \hat{n}_{z_{marginDT}} \right| \right) + \delta_e \quad (336)$$

3.4.1.2 Angle of Attack as the Critical Limit Parameter

Angle of attack is one of the fast states of the aircraft and directly estimated using an approximate model inverse and adaptive element in Eq. (327). Dynamic trim value of angle of attack is found by inserting zero to derivative terms as in Eq. (328). Steady state value of angle of attack estimation (α_{DT}) is used in limit margin calculations:

$$\hat{\alpha}_{margin} = \hat{\alpha}_{lim} - \hat{\alpha}_{DT}. \quad (337)$$

The linear relationship between control margin and limit margin is established through control sensitivity. Sensivity of angle of attack to elevator input is:

$$S_\alpha = \frac{\partial \hat{\alpha}_{DT}}{\partial \delta_e} \quad (338)$$

$$S_\alpha = -A_1^{-1}B + \left[\frac{\partial \hat{\alpha}_{DT}}{\partial \delta_e} \right]_{\dot{q}=0, \dot{\alpha}=0} \quad (339)$$

Hence, control limit becomes:

$$\hat{\delta}_{e_{lim}} = \frac{1}{S_\alpha} \hat{\alpha}_{margin} + \delta_e. \quad (340)$$

Finally, the control limits calculated in Eq. (336) and Eq. (340) are compared and the most critical one is taken as the current elevator control limit.

3.4.2 Adaptive Neural Network Augmentation with SHL Concurrent Learning

The learning algorithm for the adaptive element introduced in Eq. (326) is selected as Concurrent Learning, which is an adaptive learning scheme that uses recorded data for learning and does not require persistency of excitation [5]. Concurrent learning is used with both linear parameter neural network (LPNN) and single hidden layer neural network (SHL NN) structures in this work.

For structured uncertainties that are linearly parametrizable LPNN scheme can be used. Although the aircraft model is nonlinear and the structure of the uncertainty is not exactly known, when LPNN scheme is used weights will be bounded around the optimal weights [8]. For LPNN the adaptive element Δ can be constructed as:

$$\Delta(\bar{\mathbf{x}}) = \mathbf{W}^T \Phi(\bar{\mathbf{x}}). \quad (341)$$

where, the basis vector $\bar{\mathbf{x}}$ is selected as:

$$\Phi(i) = \phi_i(\partial(q)_d(i)), \quad i = 1 : 4 \quad (342)$$

$$\Phi(i + 4) = \phi_{i+4}(\partial(\alpha)_d(i)), \quad i = 1 : 4 \quad (343)$$

$$\Phi(9 : 12) = [\phi_9(V) \ \phi_{10}(\theta) \ \phi_{11}(\delta_e) \ b_1]^T \quad (344)$$

The activation function $\phi_i(\cdot)$ is selected as hyperbolic tangent function to ensure boundedness:

$$\phi_i(\cdot) = a_i \tanh\left(\frac{\cdot}{a_i}\right) \quad i = 1, 2, \dots, 12 \quad (345)$$

The a_i in Eq. (345) are design parameters.

Single Hidden Layer Neural Network (SHL NN) scheme is often used for continuous unstructured uncertainties. In this case exact knowledge of the uncertainty is not required. The uncertainty Δ can be constructed with SHL NN as:

$$\Delta(\bar{\mathbf{x}}) = \mathbf{W}^T \sigma(\mathbf{V}^T \bar{\mathbf{x}}) \quad (346)$$

For this problem number of single hidden layer neurons is selected as 3. Then, the synaptic weight matrix between hidden layer and output layer becomes:

$$\mathbf{W} = \begin{bmatrix} \theta_w \\ w_1 \\ w_2 \\ w_3 \end{bmatrix} \in \mathfrak{R}^{4 \times 1} \quad (347)$$

Here, θ_w is the bias and w_i are synaptic weights. Similarly, the synaptic weight matrix between input layer and hidden layer is:

$$V = \begin{bmatrix} \theta_{v,1} & \theta_{v,2} & \theta_{v,3} \\ v_{1,1} & v_{1,2} & v_{1,3} \\ \vdots & \vdots & \vdots \\ v_{12,1} & v_{12,2} & v_{12,3} \end{bmatrix} \in \mathfrak{R}^{13 \times 3} \quad (348)$$

Here, $\theta_{v,i}$ are bias and $v_{i,j}$ are synaptic weights. The input vector of SHL NN, \bar{x} is:

$$\bar{x} = \begin{bmatrix} b_v \\ x_{in} \end{bmatrix} = \begin{bmatrix} b_v \\ \partial(q)_{1_d} \\ \vdots \\ \partial(q)_{4_d} \\ \partial(\alpha)_{1_d} \\ \vdots \\ \partial(\alpha)_{4_d} \\ V_d \\ \theta_d \\ \delta_{e_d} \end{bmatrix} \in \mathfrak{R}^{12 \times 1} \quad (349)$$

Finally, the sigmoidal activation functions are in the form:

$$\sigma(z) = \begin{bmatrix} b_w \\ \sigma_1(z_1) \\ \sigma_2(z_2) \\ \sigma_3(z_3) \end{bmatrix} \in \mathfrak{R}^{4 \times 1} \quad (350)$$

where, $z = V^T \bar{x}$ and elements of σ are:

$$\sigma_i(z_i) = \frac{1}{1 + e^{-a_i z_i}} \quad (351)$$

with a_i 's as design parameters.

3.4.3 Simulation Results for Fixed Wing Aircraft Application

For simulations the aircraft is trimmed at $120kt$ forward speed and $2200m$ altitude. For this flight condition the linear model given in Eq. (325) is used with system

matrices A and B are selected as:

$$A = \begin{bmatrix} -0.5 & 6 & 0 & -10 \\ 0 & -5.5 & 0.7 & 0 \\ 0 & -8 & -8 & 0 \\ 0 & 0 & 1 & 0 \end{bmatrix} \quad B = \begin{bmatrix} -1 \\ 1 \\ 2 \\ 0 \end{bmatrix} \quad (352)$$

The positive angle of attack limit is taken as 15 deg and the positive load factor limit is taken as 3.5g. The adaptive element is modelled with SHL NN CL. The first simulation is run with pre-specified input scenario which is a sequence of pull up and push over maneuvers. Other simulations are piloted and employ different feedback cues on active side stick.

3.4.4 Case 1 : Adaptive Control Limit Estimation

This scenario is not piloted and various pitch up pitch down inputs are given in longitudinal channel. Forward speed, altitude, pitch angle and roll angle of the aircraft for the given input scenario is displayed in Fig. (3.29). Response of limit parameters, angle of attack and load factor are plotted in Fig. (3.30). In Fig. (3.31) the input scenario is shown together with control limit estimates for both load factor and angle of attack. The limit avoidance algorithm automatically selects the smaller control limit. Initially, the adaptation is OFF. SHL-Concurrent Learning scheme starts adaptation at $t = 10s$. In Fig. (3.32) adaptive weights for angle of attack and load factor are shown. Weights for both parameters are observed to converge after adaptation is turned ON. Finally, Fig. (3.33) displays model error, ξ versus adaptive element, Δ for both angle of attack and load factor. For angle of attack, adaptive element tracks model error. For load factor, adaptive element tracks model error with slight differences. This difference is acceptable and does not disturb limit avoidance performance.

3.4.5 Case 2 : Hard Stop

For this case, real time simulations are run on simulator test bench described in section 3.2. This scenario is piloted and **hard stop** feedback cue scheme is employed in

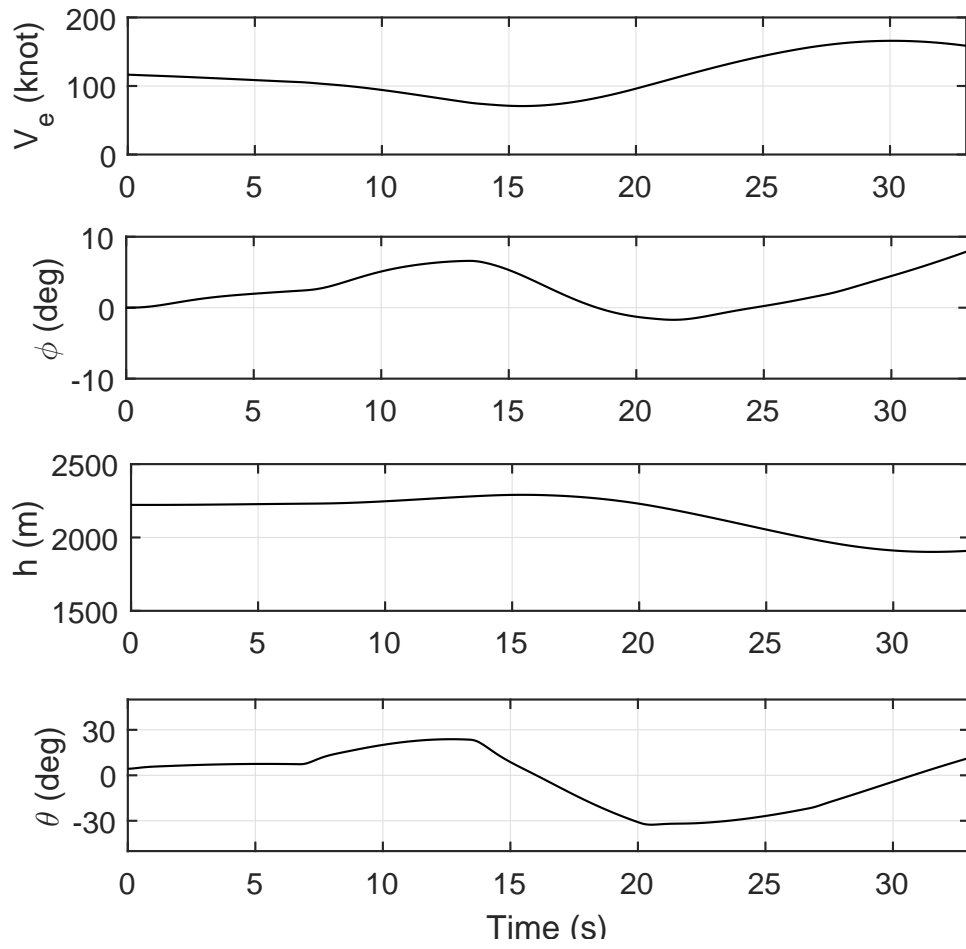


Figure 3.29: Case 1: Aircraft States

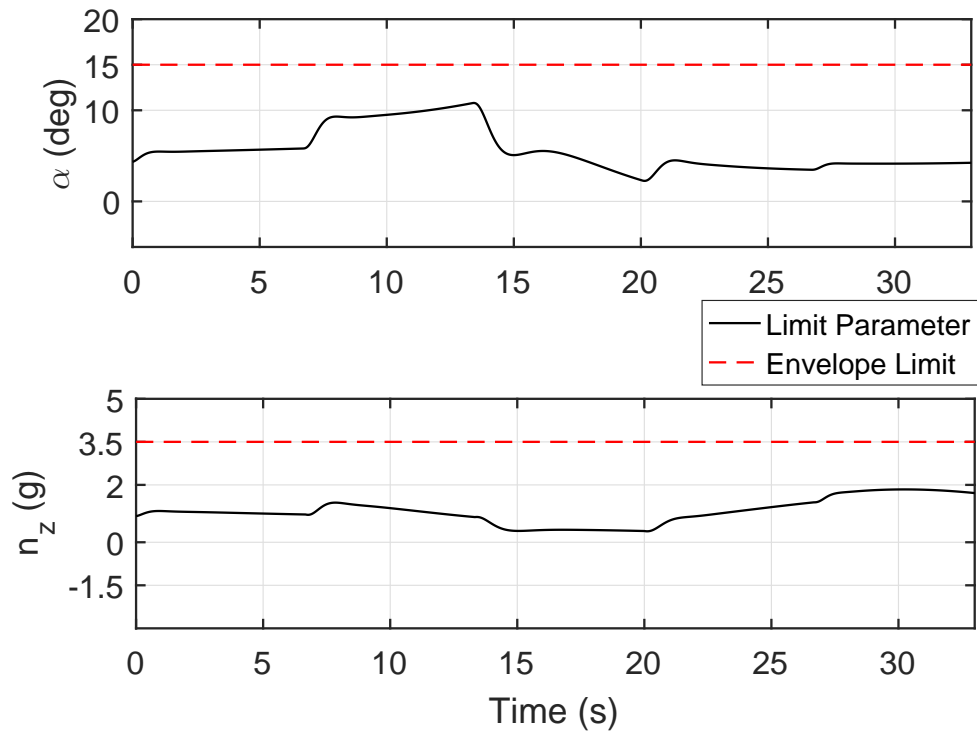


Figure 3.30: Case 1: Limit Parameters

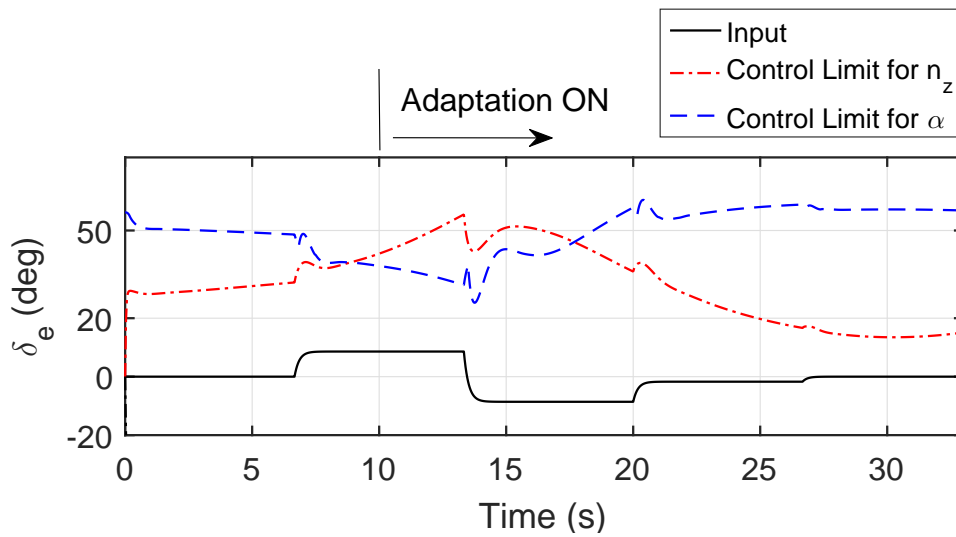


Figure 3.31: Case 1: Elevator Input and Control Limits

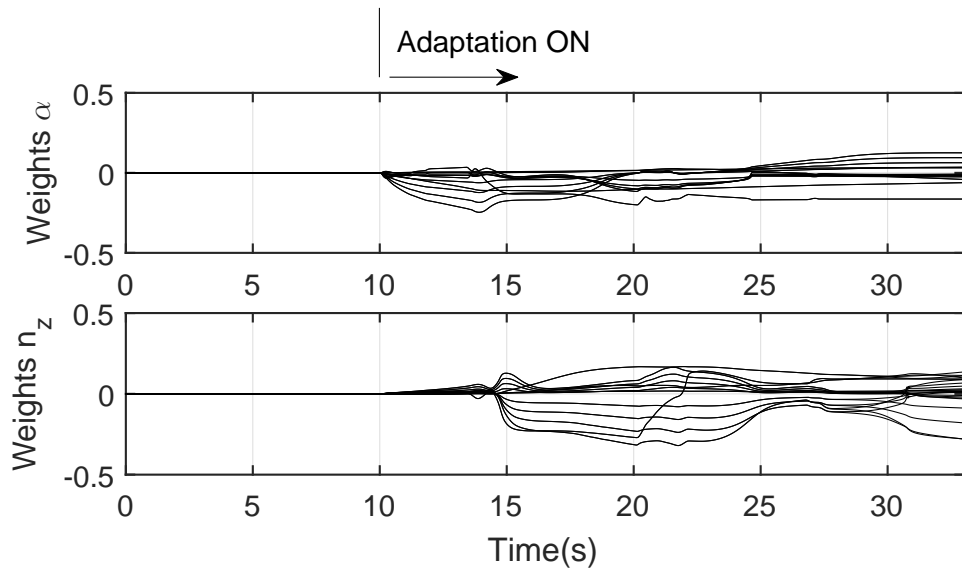


Figure 3.32: Case 1: Adaptive Weights

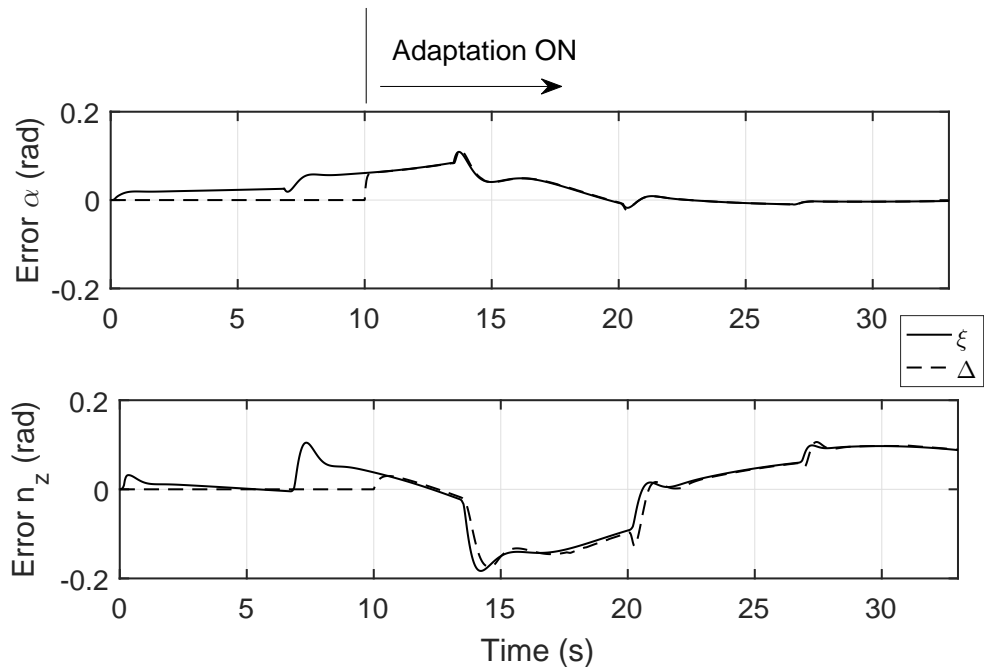


Figure 3.33: Case 1: Model Error and Adaptive Element

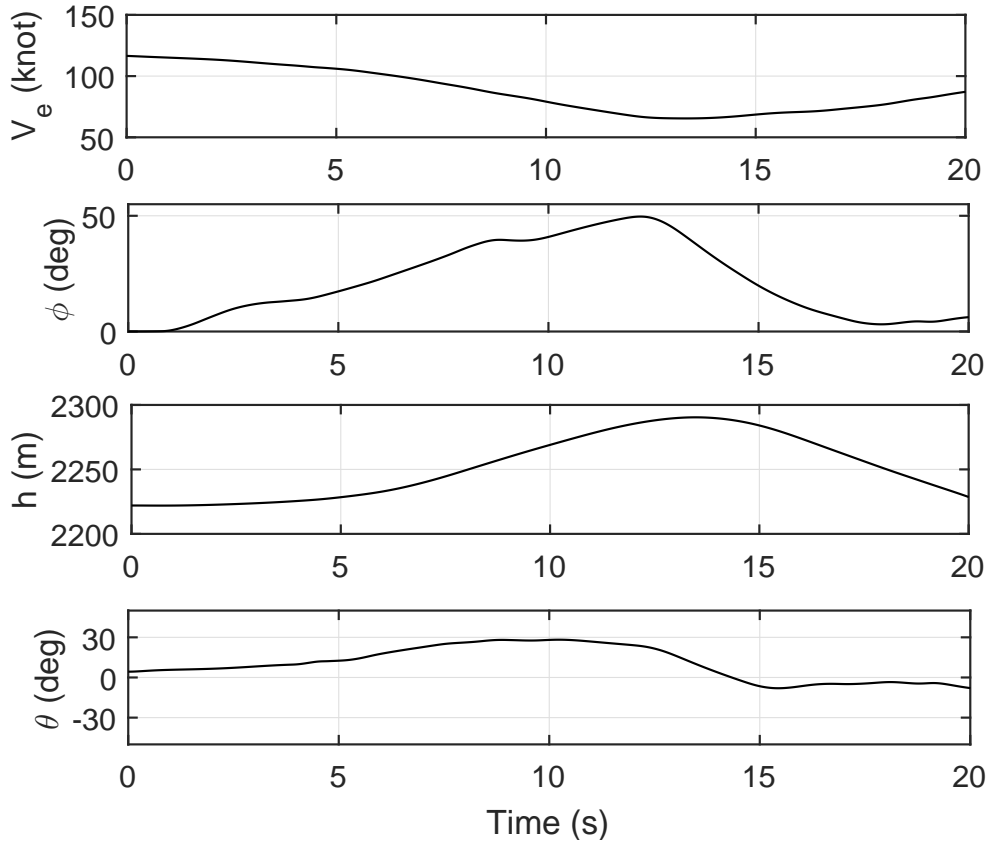


Figure 3.34: Case 2: Aircraft States for High α Turn

active side stick. At envelope limit the stick cannot move any further in limiting direction; thus, preventing the pilot from exceeding aircraft limits. For this scenario pilot performs 2 turn maneuvers: first with high angle of attack and second with high load factor.

3.4.5.1 High Angle of Attack Turn

For this maneuver, the critical limit parameter is angle of attack. In Fig. (3.34) forward speed, altitude, pitch angle and roll angle for the maneuver is displayed. Limit parameters, α and n_z are shown in Fig. (3.35). In Fig. (3.36) the input scenario is shown together with control limit estimates for both load factor and angle of attack. Fig. (3.37) shows the force feedback on the active side stick. In Fig. (3.38) adaptive weights for angle of attack and load factor are shown. Weights for both parameters are convergent. Finally, Fig. (3.39) displays model error, ξ versus

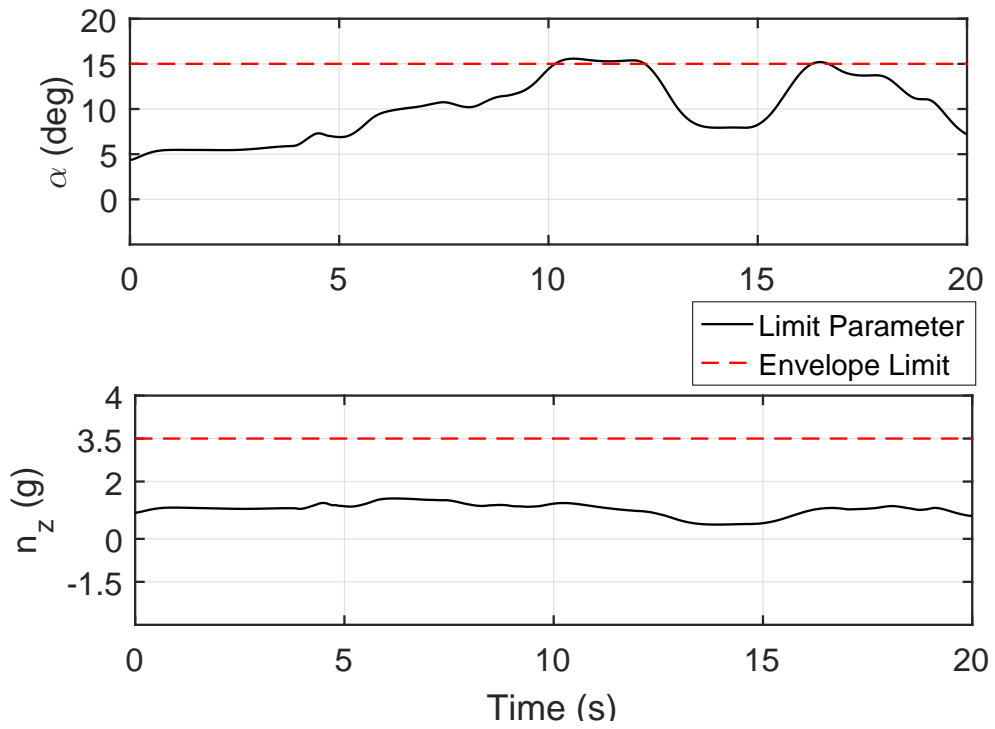


Figure 3.35: Case 2: Limit Parameters for High α Turn

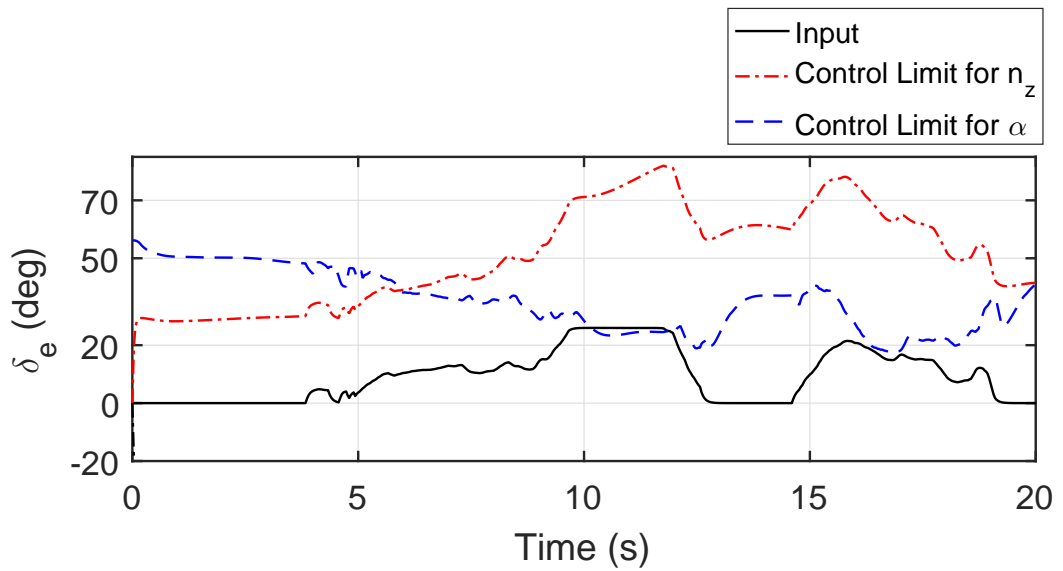


Figure 3.36: Case 2: Elevator Input and Control Limits for High α Turn

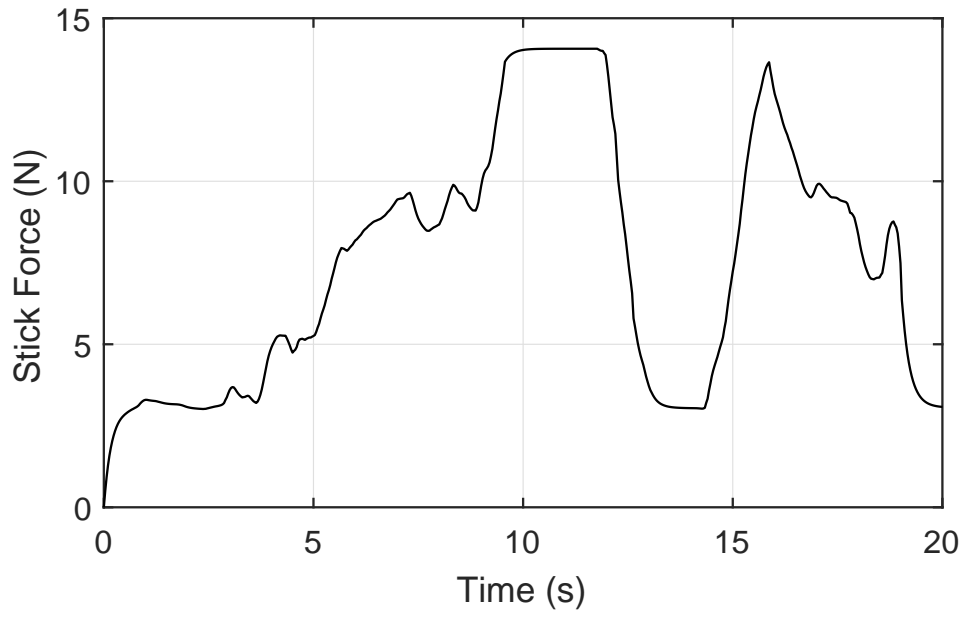


Figure 3.37: Case 2: Stick Force Feedback for High α Turn

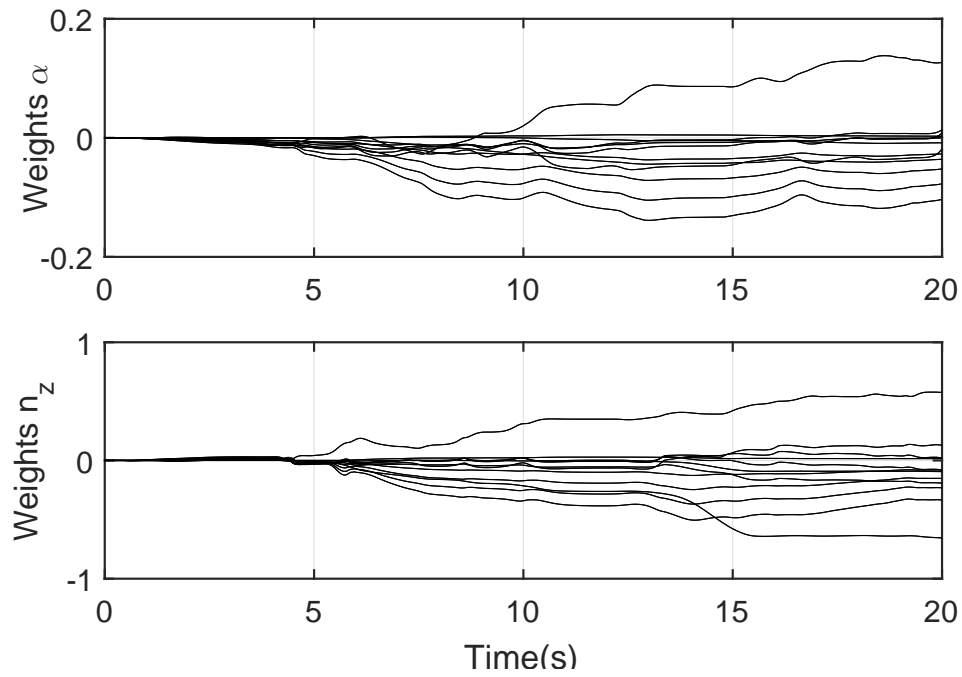


Figure 3.38: Case 2: Weights for High α Turn

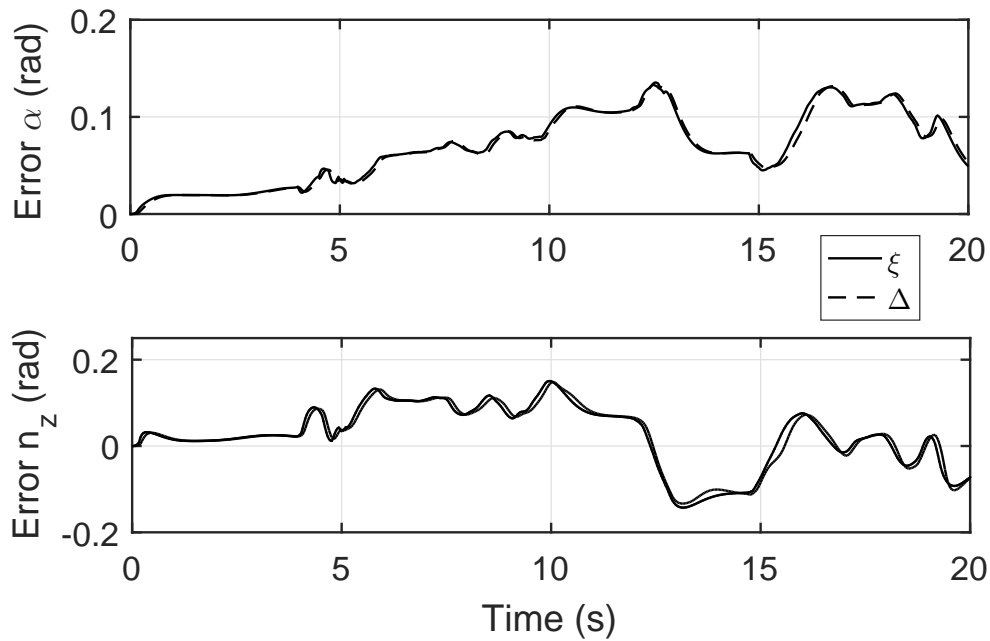


Figure 3.39: Case 2: Model Error and Adaptive Element for High α Turn

adaptive element, Δ for both angle of attack and load factor.

3.4.5.2 High Load Factor Turn

For this maneuver, the critical limit parameter is load factor. Limit parameters, α and n_z are shown in Fig. (3.40). In Fig. (3.41) the input scenario is shown together with control limit estimates for both load factor and angle of attack. Fig. (3.42) shows the force feedback on the active side stick.

3.4.6 Case 3 : Soft Stop

For this case, real time simulations are run on simulator test bench described in section 3.2. This scenario is piloted and **soft stop** feedback cue scheme is employed in active side stick. At envelope limit the stick exerts a large force to prevent the pilot from exceeding the limit. However, should the pilot chooses to exceed aircraft limits, they can overcome this force and further move the stick. Similar to previous case, for this

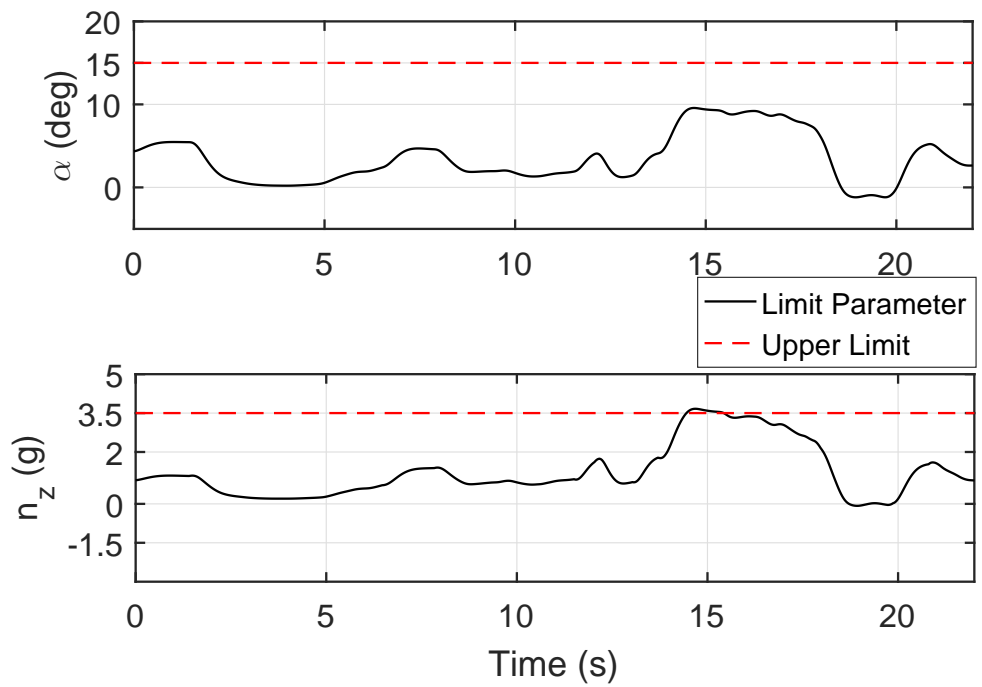


Figure 3.40: Case 2: Limit Parameters for High n_z Turn

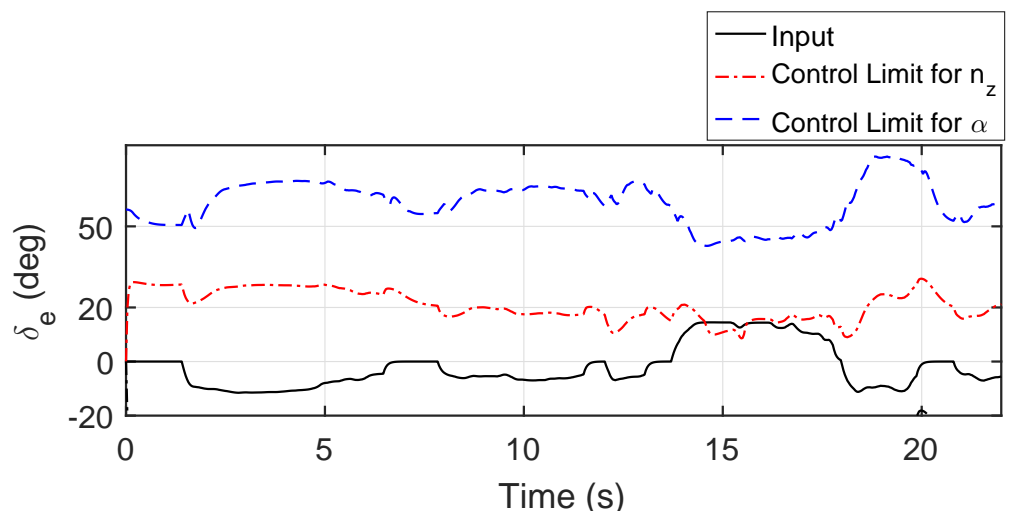


Figure 3.41: Case 2: Elevator Input and Control Limits for High n_z Turn

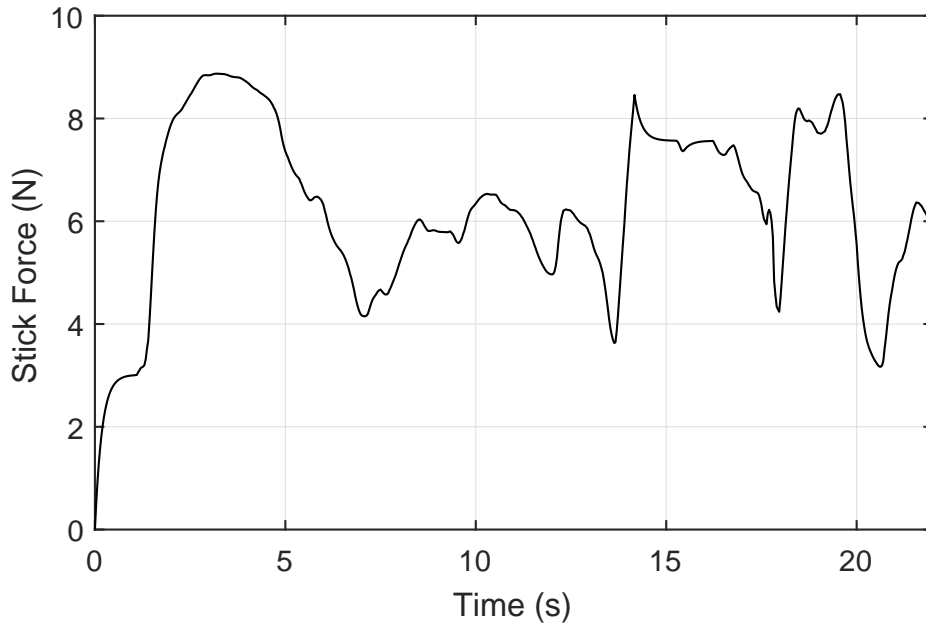


Figure 3.42: Case 2: Stick Force Feedback for High n_z Turn

scenario pilot performs 2 turn maneuvers: first with high angle of attack and second with high load factor. For both cases the pilot is stopped by the active side stick and intentionally exceeds the limits by applying a greater force to the stick.

3.4.6.1 High Angle of Attack Turn

For the first turn, critical limit parameter is angle of attack. In Fig. (3.43) forward speed, altitude, pitch angle and roll angle for the high angle of attack maneuver is displayed. Limit parameters, α and n_z are shown in Fig. (3.44). At $t = 8s$ pilot reaches the angle of attack limit and stopped by the active inceptor. Then at $t = 12s$ pilot decides to exceed the angle of attack limit by exerting a greater force. In Fig. (3.45) the input scenario is shown together with control limit estimates for both load factor and angle of attack. Fig. (3.46) shows the force feedback on the active side stick. At envelope limit, at $t = 8s$ the stick is gives a large force feedback and limit exceedance is avoided. Then the pilot starts exerting an even greater force and intentionally exceeds the angle of attack envelope limit. In Fig. (3.47) adaptive weights for angle of attack and load factor are shown. Weights for both parameters

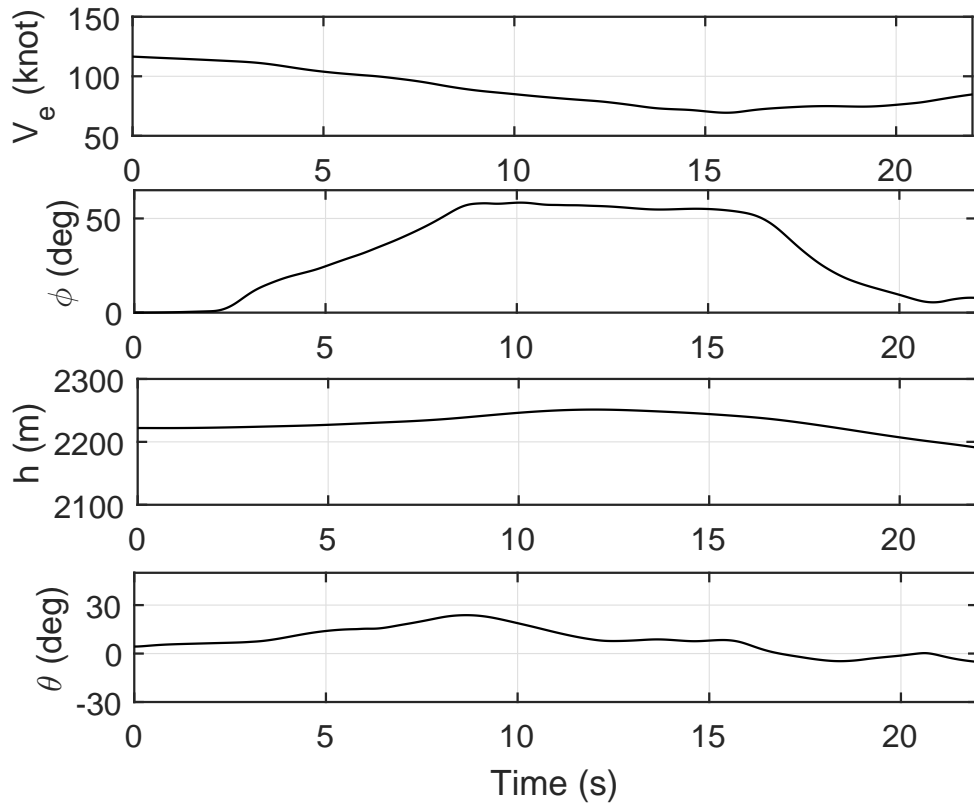


Figure 3.43: Case 3: Aircraft States for High α Turn

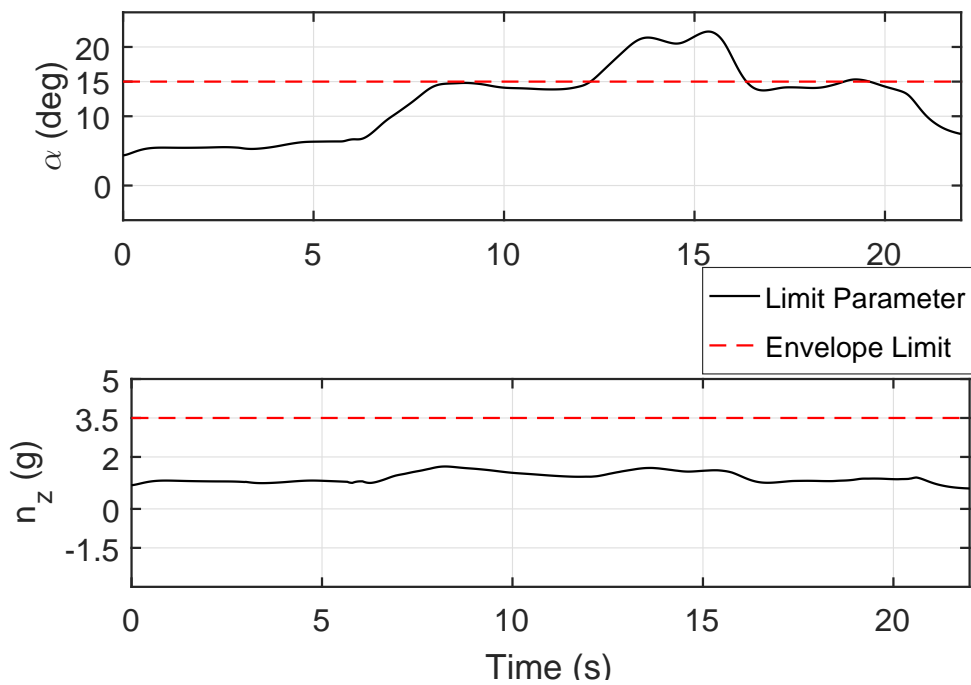


Figure 3.44: Case 3: Limit Parameters for High α Turn

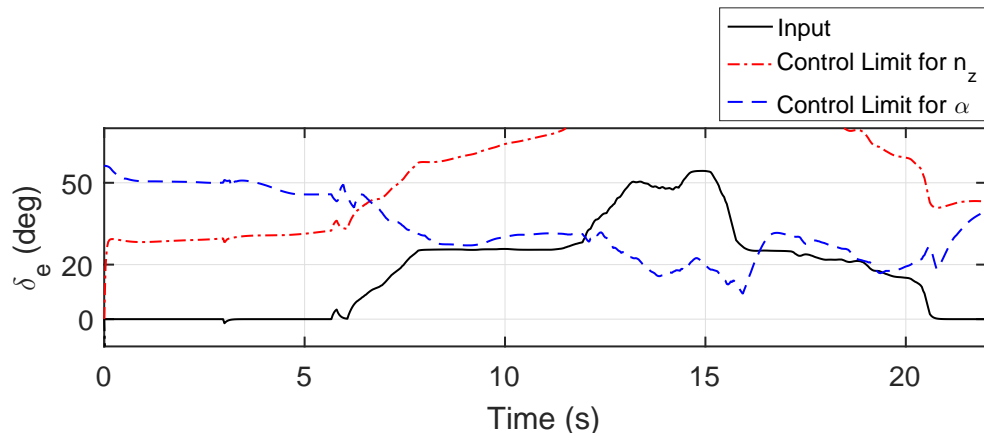


Figure 3.45: Case 3: Elevator Input and Control Limits for High α Turn

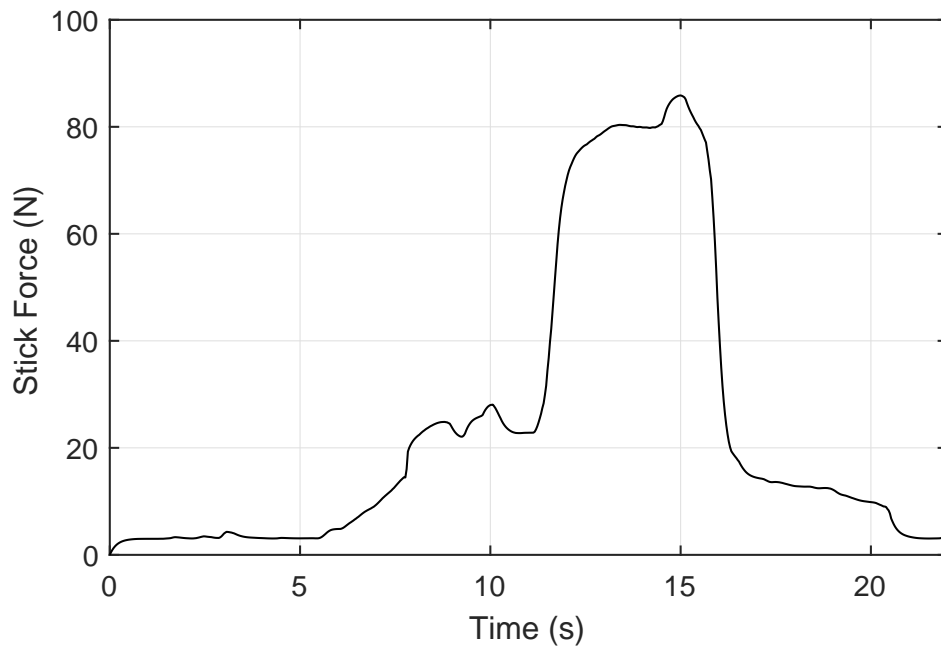


Figure 3.46: Case 3: Stick Force Feedback for High α Turn

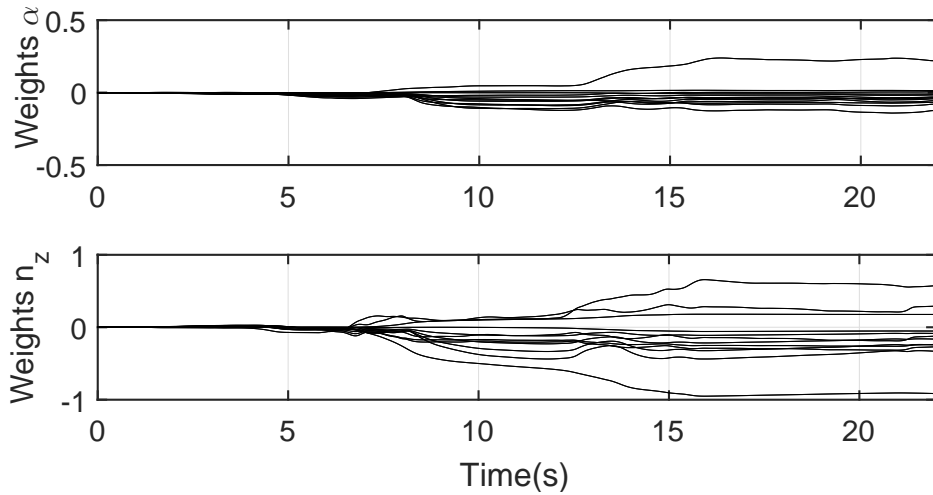


Figure 3.47: Case 3: Weights for High α Turn

are convergent. Finally, Fig. (3.48) displays model error, ξ versus adaptive element, Δ for both angle of attack and load factor.

3.4.6.2 High Load Factor Turn

For the second turn, critical limit parameter is load factor. Limit parameters, α and n_z are shown in Fig. (3.49). In Fig. (3.50) the input scenario is shown together with control limit estimates for both load factor and angle of attack. The large variation in n_z control limit is originated from use of Eq.(336). Fig. (3.51) shows the force feedback on the active side stick. At envelope limit, the stick gives a large force feedback and limit exceedance is avoided. Then the pilot starts exerting an even greater force and intentionally exceeds the load factor envelope limit.

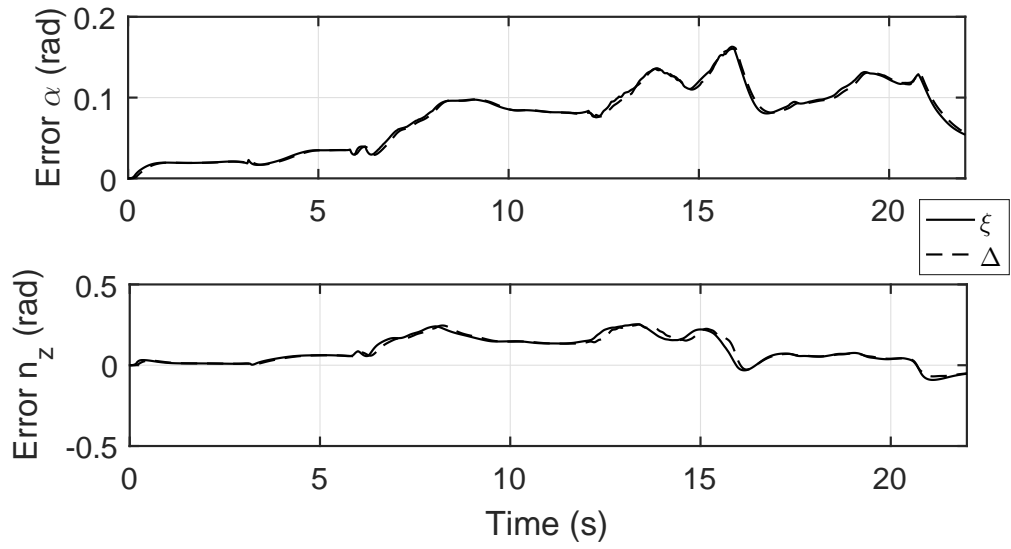


Figure 3.48: Case 3: Model Error and Adaptive Element for High α Turn

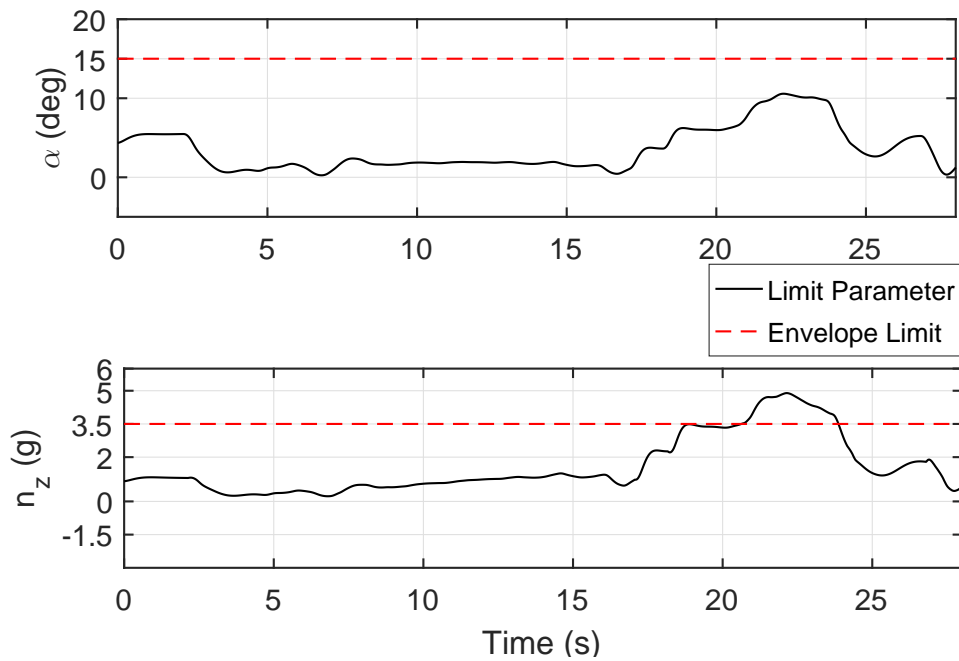


Figure 3.49: Case 3: Limit Parameters for High n_z Turn

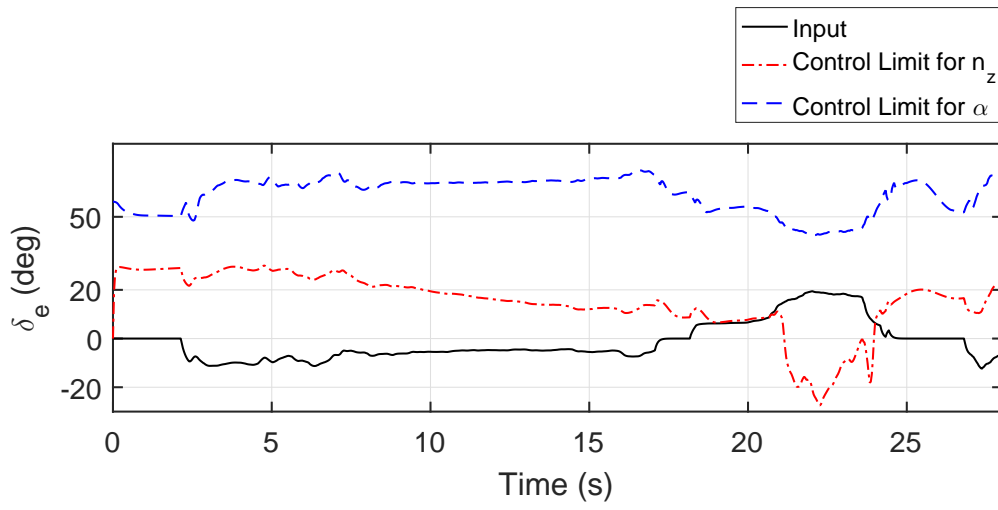


Figure 3.50: Case 3: Elevator Input and Control Limits for High n_z Turn

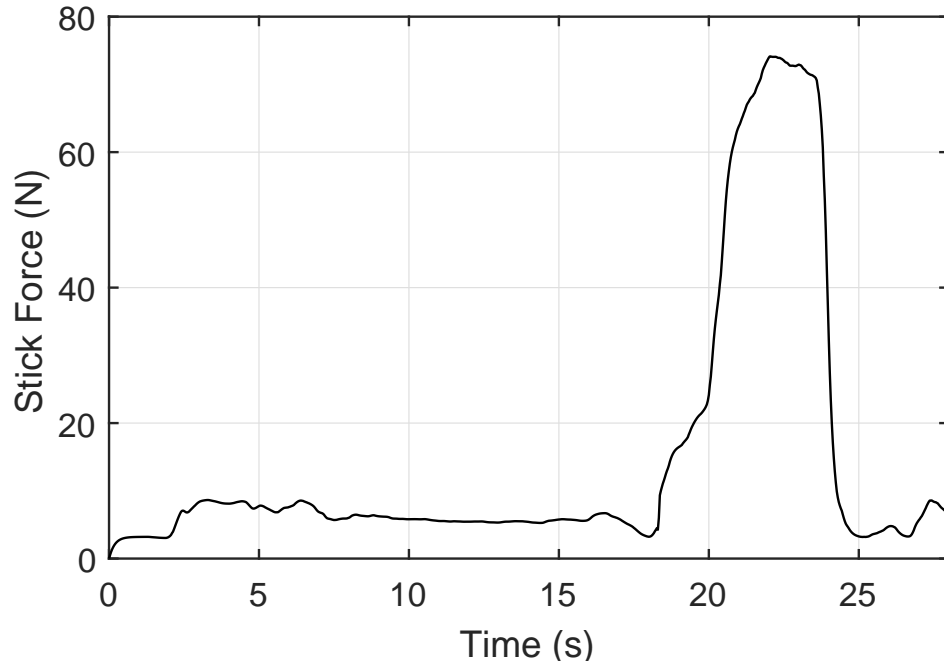


Figure 3.51: Case 3: Stick Force Feedback for High n_z Turn

CHAPTER 4

CONCLUSIONS

Limit avoidance algorithms for active side stick are studied in this thesis. An important points in limit avoidance with pilot cueing is the timely estimation of allowable control travels. For that task direct adaptive limit margin estimation method introduced in [8, 10] is employed. In that method, future values of limit parameters are estimated online as the summation of approximate inverse model and an adaptive element at dynamic trim, which is a maneuvering steady state condition. Then, limit margin is calculated using estimated future states. Using the linear relation between limit margin and control limit, control limits are calculated. Calculated limits are fed into the programmable active inceptor to produce force feedback cues. The method is tested on a simulator test bench for different force feedback maps.

The simulator test bench is proved to be sufficient for analyzing new flight envelope protection algorithms. The Stirling dynamics active side stick included in the simulations can be used for controlling lateral and longitudinal states when connected as stick or cyclic, or it can be inverted and used as collective. This versatility in configurations enables testing different algorithms for different flight envelopes. Its user friendly interface and compatibility with MATLAB Simulink allows different force feedback schemes to be designed with ease. With the ability to assign different forces to desired angles it was possible to integrate this active inceptor with proposed limit parameter estimation algorithms. Furthermore, the magnitude of the force can be tuned according to pilot need through Stirling dynamics active inceptor.

Three different nonlinear force maps are designed for this study; hard stop, soft stop, and force gradient. In hard stop method, the active inceptor is programmed to apply a very large force at limit angle such that the pilot cannot overcome the stick force and cannot move the stick any further. This force map was most effective for avoid-

ing steady state critical limit parameters like angle of attack. When the future state is accurately estimated, the hard stop acts smoothly and timely. Furthermore, it can also prevent exceeding envelope boundaries in case of aggressive inputs. However, if the dynamic trim condition is not correctly estimated, the hard stop locks the stick abruptly and cause pilot induced oscillations. In soft stop design, the inceptor is programmed to give a force feedback that is large enough for not exceeding by accident at limit angle; however, it is possible to overcome this force and move the stick further if desired. This force at the envelope limit needs to be tuned according to pilot needs and stick configuration such that; it should be large enough to prevent the pilot from exceeding the limit accidentally but should not be too large so that the pilot can still operate the aircraft after exceeding limits. Soft stop scheme acts similar to hard stop with only difference being it gives the pilot authority to exceed limits when necessary. Third design is the force gradient map. In this approach, the stick is programmed to give increasing force feedback to the pilot as control margin decreases. This method performed most effectively with peak response critical parameters like load factor response of helicopter model. Peak response critical parameters may exceed limits during transition and since transient response cannot be foreseen with the proposed method applying a force feedback at limit angle only is too late for limit avoidance. In force gradient method, force feedback on stick increases gradually and can prevent exceeding envelope limits even for peak response critical parameters. Furthermore, force gradient method is sensitive to input rate such that it reacts more aggressively in case of aggressive maneuvers. On the other hand the initial force, final force and the force increment on the stick needs to be tuned according to stick position and pilot needs. Too steep increase in force may lead to pilot induced oscillations as the pilot is surprised when the force on the stick suddenly increases. Similarly, if the force gradient is too small, limits cannot be avoided as the pilot cannot feel the change in stick force.

The adaptive element in parameter estimation algorithm is selected as linear parameter neural network (LPNN) and single hidden layer neural network (SHL NN). Weight update law for both neural network schemes are selected as concurrent learning algorithm (CL). Concurrent learning uses both current data and recorded past data for learning. Concurrent learning guarantees convergence to optimal weights and optimal weights are required for dynamic trim estimations. If the weights are not optimal

the dynamic trim cannot be correctly calculated even if the neural networks compensate for the model error and weights converge to some value. For slow maneuvers near trim condition, both neural networks act similarly, and successfully estimate the model error. This is because the basis of the LPNN can estimate the uncertainty in that linear region. However, errors in SHL NN is less than LPNN for aggressive maneuvers and when there are deviations from linear model at trim condition since SHL NN can solve unstructured uncertainties. Since LPNN cannot estimate the critical parameters accurately without the correct basis vector and it is not always possible to construct a basis that expresses the uncertainty in model perfectly, using SHL NN bears more accurate estimations.

As future work, the performance of SHL NN CL in different flight conditions can be improved by application of purging algorithms that erase irrelevant data from the history stack. Some other adaptive learning schemes in literature such as concurrent learning with random basis functions (RBF CL) or concurrent learning with reinforced learning can be applied as the adaptive element in direct adaptive limit margin estimation method. Variety of force feedback map designs can be increased; existing methods can be combined or stick shakers can be added. Evaluation of both limit margin estimation method and tactile cue designs can be tested with pilots on simulator environment.

To conclude, a simulator environment is set and proved to be sufficient for analyzing new envelope protection algorithms. The adaptive learning performance of the given method [10] is enhanced with SHL NN CL augmentation. Results are compared with LPNN CL. Performance of SHL NN is found superior for model error compensation and parameter estimation. The active inceptor is enabled to provide different force feedback cues and various force maps are designed and tested on simulator. Hard stop and soft stop performed better on steady state critical limit parameters whereas, for peak response critical parameters force gradient method provided better limit avoidance.

REFERENCES

- [1] Flight link. *www.flightlink.com*, n.d.
- [2] Saitek. *www.saitek.com*, n.d.
- [3] Stirling dynamics. *www.stirlingdynamics.com*, n.d.
- [4] A. Bateman, D. Ward, R. Barron, and M. Whalley. Piloted simulation evaluation of a neural network limit avoidance system for rotorcraft. August, 1999.
- [5] G. Chowdhary. *Concurrent Learning for Convergence in Adaptive Control Without Persistency of Excitation*. PhD thesis, Gerogia Institute of Technology, 2010.
- [6] S. Corps. Airbus a320 side stick and fly by wire-an update. *In proceedings of the SAE 5th Aerospace Behavioral Engineering Technology Conference*, Long Beach, CA., 1987.
- [7] P. Einthoven, D. Miller, J. Nicholas, and S. Margetich. Tactile cueing experiments with a three axis sidestick. *Proceedings of the American Helicopter Society 57th Annual Forum*, May 2001.
- [8] G. Gursoy. *Direct Adaptive Flight Envelope Protection*. PhD thesis, Middle East Technical University, 2016.
- [9] G. Gursoy and I. Yavrucuk. Concurrent learning enabled adaptive limit detection for active pilot cueing. *Journal of Aerospace Information Systems*, Vol:11, pp:542–550, 2014.
- [10] G. Gursoy and I. Yavrucuk. Direct adaptive limit and control margin estimation with concurrent learning. *Journal of Guidance, Control, and Dynamics*, Vol:39, No:6, pp:1356–1373, 2016.

- [11] J. Horn, A. Calise, and J. V. R. Prasad. Flight envelope cueing on a tilt-rotor aircraft using neural network limit prediction. *Journal of the American Helicopter Society*, Vol:46, pp:23–31, Jan, 2001.
- [12] J. Horn, A. Calise, and J. V. R. Prasad. Flight envelope limit detection and avoidance for rotorcraft. *Journal of the American Helicopter Society*, Vol:47, pp:253–262, October, 2002.
- [13] In Proceedings of the Thirty-Sixth European Rotorcraft Forum. *A New Helicopter Simulation and Analysis Tool: Helidyn+*. Paris, France, 9 2010.
- [14] G. J. Jeram. Open design for helicopter active control systems. *Proceedings of the American Helicopter Society 58th Annual Forum*, June 2002.
- [15] B. D. Kothmann and J. Armbrust. Rah-66 comanche core afcs control law development: Demval to emd. *Proceedings of the American Helicopter Society 58th Annual Forum*, June 2002.
- [16] J. R. Mayo and V. N. Iannacci. The rah-66 comanche flight envelope cueing system. *Proceedings of the American Helicopter Society 55th Annual Forum*, May 1999.
- [17] P. K. Menon, V. R. Iragavarapu, and M. S. Whalley. Estimation of rotorcraft limit envelopes using neural networks. *Proceedings of the American Helicopter Society 52nd Annual Forum*, June 1996.
- [18] Proceedings of the American Helicopter Society 71th Annual Forum. *Non-Iterative Adaptive Vertical Speed Limit and Control Margin Prediction for Fly-By-Wire Helicopter*. AHS International, 5 2015.
- [19] M. Rauw. *A SIMULINK environment for Flight Dynamics and Control analysis - application to the DHC-2 'Beaver'*. PhD thesis, Delft University of Technology, 1993.
- [20] O. Sensburg, O. Bartsch, and H. Bergmann. Reduction of the ultimate factor by applying a maximum load concept. *Journal of Aircraft*, Vol:24, No:11, pp:759–767, 1987.

- [21] O. Sensburg, G. Schmidinger, and K. Fuellhas. Integrated design of structures. *Journal of Aircraft*, Vol:26, No:3, pp:260–270, 1989.
- [22] D. Sun and N. Hovakimyan. A bank angle protection method based on potential functions for nonlinear aircraft model. *In proceedings of 17th AIAA Aviation Technology, Integration, and Operations Conference*, June 2017.
- [23] D. Sun, X. Li, H. Jafarnejadsani, and N. Hovakimyan. A flight envelope protection method based on potential functions. *In proceedings of AIAA Aviation Guidance, Navigation, and Control Conference*, January 2017.
- [24] M. S. Whalley and M. Achache. Joint u.s. france investigation of helicopter flight envelope limit cueing. *Proceedings of the American Helicopter Society 52nd Annual Forum*, June 1996.
- [25] M. S. Whalley, W. S. Hidson, and G. G. Thiers. A comparison of active sidestick and conventional inceptors for helicopter flight envelope tactile cueing. *Proceedings of the American Helicopter Society 56th Annual Forum*, May 2000.
- [26] I. Yavrucuk. *Adaptive Limit Margin Detection and Limit Avoidance*. PhD thesis, Georgia Institute of Technology, 2003.
- [27] I. Yavrucuk and J. V. R. Prasad. Online dynamic trim and control limit estimation. *Journal of Guidance, Control, and Dynamics*, Vol:35, No:5, pp:1647–1656, 2012.